Ocean Engineering 257 (2022) 111653

Contents lists available at ScienceDirect

Ocean Engineering

journal homepage: www.elsevier.com/locate/oceaneng

Seismic response of large offshore wind turbines on monopile foundations including dynamic soil–structure interaction

Luis A. Padrón [a,*], Sandro Carbonari [b], Francesca Dezi [c], Michele Morici [d], Jacob D.R. Bordón [a], Graziano Leoni [d]

[a] University Institute of Intelligent Systems and Numerical Applications in Engineering (SIANI), Universidad de Las Palmas de Gran Canaria, Spain
[b] Department of Construction, Civil Engineering and Architecture (DICEA), Università Politecnica delle Marche, Italy
[c] Geology Division, School of Science and Technology, University of Camerino, Italy
[d] School of Architecture and Design (SAAD), University of Camerino, Italy

ARTICLE INFO

Keywords:
Offshore wind turbines
Earthquake response
Soil–structure interaction
Lumped parameter models
OpenFAST

ABSTRACT

This paper presents the results of a study on the dynamic and seismic response of the support structures of three reference Offshore Wind Turbines (OWT) of increasing rated power, founded to the seabed through monopile foundations. Thus, the structural behaviour of the NREL 5 MW, IEA Wind 10 MW and IEA Wind 15 MW reference OWTs under seismic input is analysed. To do so, a model based on the aero-hydro-servo-elastic OpenFAST open-software code, modified to include dynamic Soil–Structure Interaction (SSI) and input ground motion, is employed. Dynamic SSI phenomena are incorporated through lumped parameter models fitted to the impedances computed using an advanced boundary elements–finite elements model of the soil–foundation system in which the monopile is discretized as a steel pipe buried in the unbounded seabed. The fore–aft and side-to-side responses of the systems are computed under power production, parked and emergency shutdown operating conditions considering different earthquakes and arrival times. It is found that even low and moderate intensity earthquakes can produce significant increases in the structural demands of large OWTs. There exists a clear tendency for SSI to be beneficial when the size of the OWT increases.

1. Introduction

The installed capacity of electric power generation from offshore wind has been growing significantly in the last decades. Most of the Offshore Wind Turbines (OWT) installed in Europe are located in places where the depth of the sea allows founding them directly to the seabed. In fact, the average water depth in wind farms under construction in Europe during 2019 was 33 m, with an average distance to the coast of 59 km, and even though floating technology is developing fast, 70% of wind turbines newly-installed were founded on monopiles, and 29% on jacket substructures (EWEA, 2020).

The size and rated power of the turbines have been constantly increasing, leading to larger machines, with longer blades and higher towers. In fact, wind turbines have increased from initial diameters of 30 m, hub heights of 30 m and rated powers of 300 kW; to diameters of 125 m and rated powers of 5 MW only a few years ago; to the present turbines of around 10 MW, as for instance, the 9.5 MW V164-9.5 with a diameter of 164 m and hub heights over 100 m, and with more powerful wind turbines already on their way. This increasing rated power implies that the impact of the downtime due to failure or maintenance of one unit would be much higher, which leads to the need of reducing the risk of failure, given that failure rates and downtimes due to maintenance could rapidly counterbalance the benefits of these large turbines (Hofmann and Sperstad, 2014).

At the same time, the growing demand for offshore wind technology implies that the installation of new offshore wind farms in locations with technically less favourable geological and geotechnical conditions, greater water depths and/or increasing seismic risk will be increasingly interesting. Current standards and design guidelines state that earthquake resistance should be demonstrated for locations where seismic loads might be critical (IEC, 2005; DNV, 2014), but the experience in this field is limited because the technology is relatively recent, and many of the studies on the seismic response of wind turbines that can be found in the literature are made on turbines with sizes and rated powers smaller than those dominant today.

A pioneering work on the seismic response of wind turbines is that of Bazeos et al. (2002), in which a prototype with an almost 38 m

* Corresponding author.
E-mail addresses: luis.padron@ulpgc.es (L.A. Padrón), s.carbonari@staff.univpm.it (S. Carbonari), francesca.dezi@unicam.it (F. Dezi), michele.morici@unicam.it (M. Morici), jacobdavid.rodriguezbordon@ulpgc.es (J.D.R. Bordón), graziano.leoni@unicam.it (G. Leoni).

https://doi.org/10.1016/j.oceaneng.2022.111653
Received 28 November 2020; Received in revised form 11 May 2022; Accepted 26 May 2022
Available online 10 June 2022

high steel tower was analysed using three different structural models: a refined three-dimensional model in which the tower was discretized using shell finite elements; a simplified multi-degree of freedom beam model; and a one degree-of-freedom oscillator in the form of a cantilever with a concentrated mass at its free end. The study, that was performed in time domain and also using spectral analysis, revealed two interesting conclusions for this case of study: that the three models yielded comparable results in terms of the studied seismic variables; and that the stress generated by the seismic actions were, in this case, much smaller than those produced by extreme wind events. Almost simultaneously, Lavassas et al. (2003) presented a similar analysis on a slightly larger wind turbine, 44 m high, obtaining similar conclusions regarding the prevalence of wind loads over the seismic actions in these initial wind turbines. However, some time later, when studying the seismic response of a taller wind turbine, already 70 m high, through a finite elements model, Wang and Zhang (2011) concluded that seismic actions could be the dominant factor in the design of the support structure.

Thereafter, the relevance of the seismic actions on the structural systems of the wind turbines has also been highlighted by a significant number of authors (Prowell, 2011; Wang and Dong, 2011; Stamatopoulos, 2013; Song et al., 2013; Prowell et al., 2014; Díaz and Suárez, 2014; Valamanesh and Myers, 2014; Kim et al., 2014; Damgaard et al., 2014b, 2015a; Mardfekri and Gardoni, 2015; Asareh et al., 2015; Kjørlaug and Kaynia, 2015; Anastasopoulos and Theofilou, 2016; Asareh et al., 2016a,b; Santangelo et al., 2016; Sadowski et al., 2017; De Risi et al., 2018; Ju and Huang, 2019; Ali et al., 2020). However, not all of these studies considered the influence of Soil–Structure Interaction (SSI) phenomena, even though many researchers have already proven that such interaction modifies the dynamic response of the system (Bhattacharya and Adhikari, 2011; Andersen et al., 2012; Harte et al., 2012; Lombardi et al., 2013; Zania, 2014; Carswell et al., 2015a; Ghaemmaghami et al., 2017; Álamo et al., 2018). Also, the foundation dynamic characteristics, in terms of stiffness (and its influence on the natural frequencies) and in terms of the capacity to dissipate energy (through radiation damping), play a fundamental role in the overall dynamic and seismic response of the support structure and in the reduction of the accumulated damage.

Relevant studies that have taken into account soil–structure interaction phenomena to analyse the seismic response of wind turbines are, for instance, those of Bazeos et al. (2002), Stamatopoulos (2013), Damgaard et al. (2013), Mardfekri and Gardoni (2013), Bisoi and Haldar (2014), Kjørlaug and Kaynia (2015), Mardfekri and Gardoni (2015), Alati et al. (2015), Mo et al. (2017), De Risi et al. (2018), Ju and Huang (2019), Yang et al. (2019a,b) or Ali et al. (2020). Bazeos et al. (2002) did so by introducing a matrix of constant springs and dashpots at the base of the tower, together with the consideration of added masses to simulate the soil. Thereafter, other authors such as Stamatopoulos (2013) or Alati et al. (2015), included linear or non-linear springs and dashpots in the structural models. On the other hand, instead of using springs and dashpots at the base, authors such as, for instance, Kjørlaug and Kaynia (2015) built a 3-D finite element model that included a portion of the near-field soil together with the foundation and the structure, while other studies considered the use of nonlinear Winkler p-y, t-z and Q-z springs, such as in the case of the work by Ju and Huang (2019). Lumped Parameter Models (LPM) have also been used to incorporate soil–structure interaction to models for the study of the dynamic analysis of offshore wind turbine structures. Damgaard et al. (2014a) used this approach for the study of the behaviour of a 5 MW OWT, and Carswell et al. (2015b) used it to investigate the effect of foundation damping on the structural response of OWTs. Later, Damgaard et al. (2015b) implemented it into the aero-hydro-elastic code HAWC2 to perform a probabilistic study of fatigue in monopiles under environmental loads. None of these studies considered seismic actions, but later, Taddei et al. (2017) employed an uncoupled approach to look into the dynamic response of the reference 5 MW onshore wind turbine under seismic actions using a model in which the soil–foundation subsystem was taken into account through an LPM.

The analysis of the existent literature shows that there exists a need to further understanding the seismic response of present and future offshore wind turbines founded on the seabed, so that structural and control systems can be optimally designed, and failures due to earthquake action can be avoided. For this reason, this paper aims at contributing to this topic, paying especial attention to the behaviour of the very large wind turbines that are already being built today and that are planned for the future, by studying the dynamic and seismic response of the available 10 and 15 MW reference offshore wind turbines, for which nearly no studies are yet available, in addition to the 5 MW reference turbine. Thus, the influences of soil–structure interaction, earthquake intensity, turbine rated power, operating conditions, and time of arrival of the earthquake, on the dynamic and seismic response of 5, 10 and 15 MW reference offshore wind turbines on monopiles, are studied in this manuscript. To do so, a model based on the aero-hydro-servo-elastic OpenFAST open-software code, modified to include dynamic soil–structure interaction and input ground motion, is employed. The dynamic response of the monopile foundations are incorporated by LPMs at mudline, which allows taking into account the frequency-dependent nature of the impedance functions, as well as the energy dissipated through the soil–foundation system. Previously, the impedance functions of the soil–foundation systems are computed using an advanced boundary-element finite-element model in which the monopile is modelled as a steel pipe discretized using shell finite elements, and the soil is considered as an unbounded viscoelastic region through a boundary elements discretization.

It has been found that the influence of dynamic soil–structure interaction can be beneficial or detrimental, depending on the specific case, but that it tends to be more beneficial when the size and rated power of the OWT increases. It is also shown that even low or moderate intensity earthquakes can produce significant increases in the structural demands of large offshore wind turbines in terms of accelerations at the top and of bending moments and shear forces at mudline, with bending moments in the fore–aft direction experiencing the less pronounced increases. It is also concluded that the best strategy to follow during an earthquake (triggering an emergency stop, or continuing in power production if possible, for instance) is not clear a priori, with aspects such as aeroelastic damping playing a very significant role.

The manuscript is structured in five sections. After this introduction, Section 2 describes the three offshore wind turbines that are going to be considered, and defines the ground motions, the operating modes, and the whole set of cases that are simulated in this study. Then, Section 3 presents the methodology and the models used to perform the analyses. A synthesis of the results is presented and explained in Section 4. Finally, a summary of the main conclusions drawn from the present study is presented in Section 5.

2. Problem cases description

2.1. Reference wind turbines

In order to achieve the aims described above, the following three reference wind turbines are considered in this study: (a) The NREL 5 MW reference turbine, as defined through the Offshore Code Comparison Collaboration (OC3) and as described, for instance, in Jonkman and Musial (2010) ;(b) The IEA-10.0-198-RWT reference wind turbine, as defined in Bartolotti et al. (2019); and (c) and the IEA-15-240-RWT reference wind turbine as defined in Gaertner et al. (2020). For the present study, the three offshore wind turbines are assumed as fixed-bottom to the sea floor through monopile supports, as illustrated in Fig. 1, where the main design parameters are represented to scale. The main properties of the wind turbines, together with water depth, key geotechnical parameters and monopile general properties are summarized in Table 1. Structural components of the towers and monopiles

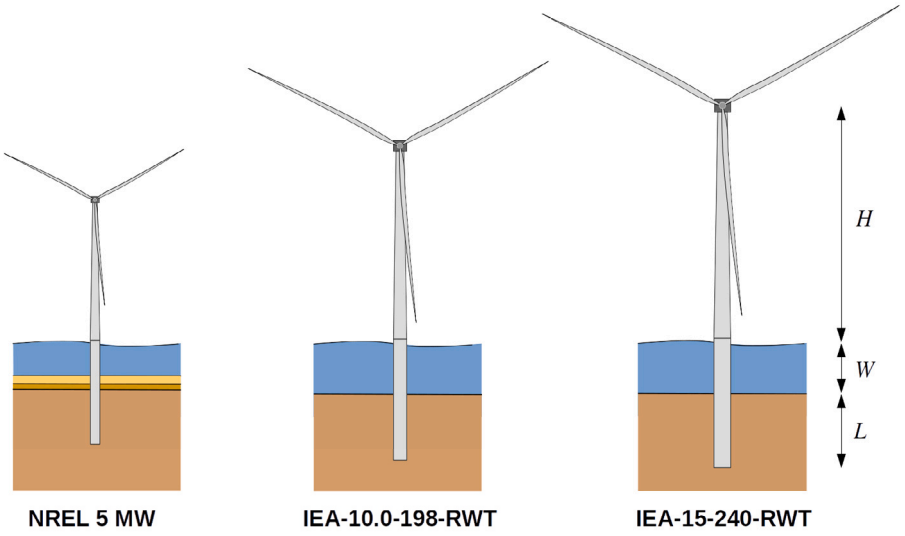

Fig. 1. Representation of the three reference wind turbines under study. Main design parameters are represented approximately to scale.

Table 1
Key parameters of the reference wind turbines considered in this study.

	NREL 5 MW	IEA-10.0-198-RWT	IEA-15-240-RWT
Rating [MW]	5	10	15
Rotor diameter [m]	126	198	240
Hub height (H) [m]	90	119	150
RNA mass [ton]	350	686	1017
Tower mass [ton]	348	628	860
Tower top diameter [m]	3.87	5.5	6.5
Tower base diameter [m]	6.0	8.3	10.0
Tower top thickness [mm]	19	31.6	24.0
Tower base thickness [mm]	27	71.1	36.5
Water depth (W) [m]	20	30	30
Pile diameter (d) [m]	6.0	9.0	10.0
Pile thickness (t) [mm]	60	101.5	55.3
Pile depth (L) [m]	36.0	42.6	45
L/d [–]	6.00	4.73	4.50

Table 2
Steel material properties.

	NREL 5 MW	IEA-10.0-198-RWT	IEA-15-240-RWT
Young's modulus, E [GPa]	210	210	200
Shear modulus, G [GPa]	80.8	80.8	79.3
Density, ρ [kg/m^3]	8500	8500	7850
Damping, ζ [–]	0.02	0.02	0.02

are assumed to behave elastically and the mechanical properties are reported in Table 2. In all cases, the value of the modal structural damping ratios is set to 1% for the first and second modes in each direction. For more information, including the detailed description of the support structures, please refer to the references given above.

The seabed properties are provided in Table 3. The ground properties corresponding to the NREL 5 MW case are extracted from Løken and Kaynia (2019), and the properties for the IEA-15-240-RWT case are obtained from Gaertner et al. (2020). In the case of the IEA-10.0-198-RWT the tower foundation is assumed to be embedded in a sandy deposit with constant properties derived from Velarde and Bachynski (2017). In particular, the unloading/reloading stiffness, E_{ur}, was taken as the static stiffness modulus, E_s, and then the shear modulus, G_s, was derived by means of the correlation provided by Alpan (1970).

2.2. Definition of the seismic input ground motions

The seismic input is defined according to ISO 19901-2 (2007) considering a medium hazard on the basis of the maps available in annex B of the code, which provides 5% damped spectral response accelerations at 0.2 and 1.0 s for most of the offshore areas of the world. Accelerations have an average return period (T_R) of 1000 years and are used to define the design response spectrum according to the simplified seismic action procedure foreseen by the code for low structure's Seismic Risk Categories (SRC2 and SRC3). The SRC depends on the structure's exposure Level (L), ranging between 1 and 3, and the seismic zone, which varies from 0 to 4 and is defined on the basis of the spectral response acceleration at 1.0 s. In detail, the site seismic zone 0 is characterized by a spectral acceleration lower than 0.03 g while the zone 4 is associated to accelerations higher than 0.45 g. In this work a SRC2 is selected in order to avoid the need of a site-specific seismic hazard assessment; the latter is compatible with the exposure level L2 and the site seismic zone 2 (characterized by a spectral acceleration at 1.0 s in the range 0.11–0.25 g). In detail, spectral response accelerations $S_{a,map}(0.2) = 0.5$ g and $S_{a,map}(1.0) = 0.2$ g at 0.2 s and 1.0 s, respectively, are considered in the applications. Values are representative of a moderate seismic hazard, consistently with the hypothesis of linear structural behaviour.

According to the simplified seismic action procedure, the site 1000 years horizontal acceleration spectrum is constructed through simple formulas accounting for the site class, which may be defined in terms of average soil shear wave velocity $V_{s,30}$ in the top 30 m of the effective seabed; in this work a site class D, presenting $V_{s,30}$ values ranging between 180 and 350 m/s, is adopted, consistently with the soil profiles hypothesized for the OWTs. The site 1000 years response spectrum is scaled by the factor 1.15 (defined by the code for the structure's exposure level L2) to obtain the response spectrum associated to the Abnormal Level Event (ALE), which is defined as an intense earthquake with a very low probability of occurrence during the structure's design service life. The ALE can cause structural damage, but the overall integrity must be assured, avoiding collapses that may cause loss of life or environmental damage. Starting from the ALE response spectrum, the Extreme Level Event (ELE) response spectrum can be defined through an overall scale factor that considers the seismic reserve capacity strength of the structure. Above factor, defined in ISO 19902 (2007), is assumed to be 2.4 in this work and represents the ratio of the spectral acceleration causing catastrophic system failure of the structure, to the ELE spectral acceleration, for which the structure should behave linearly (with little or no damage). The ELE spectrum defines a seismic action characterized by a return period of 100 years.

By considering the seismic intensities in terms of spectral accelerations relevant to return periods of 100 and 1000 years, and the relevant

Table 3
Dynamic properties of the different soil deposits.

	NREL 5 MW	IEA-10.0-198-RWT	IEA-15-240-RWT
Soil profile	layered	single layer	single layer
Type of soil	sand	sand	dense sand or gravel
Poisson's ratio, ν_s [–]	0.35	0.30	0.40
Density, ρ_s [kg/m^3]	2000	2000	2000
Shear modulus, G_s [MPa]	42.6 ($0 < z < 5$ m) 61.9 ($5 < z < 14$ m) 87.4 ($14 < z < \infty$)	92.3 ($0 < z < \infty$)	140.0 ($0 < z < \infty$)
Shear wave velocity, v_s [m/s]	145.9 ($0 < z < 5$ m) 175.9 ($5 < z < 14$ m) 209.0 ($14 < z < \infty$)	214.8 ($0 < z < \infty$)	264.5 ($0 < z < \infty$)
Damping, ζ_s [–]	0.05	0.05	0.05

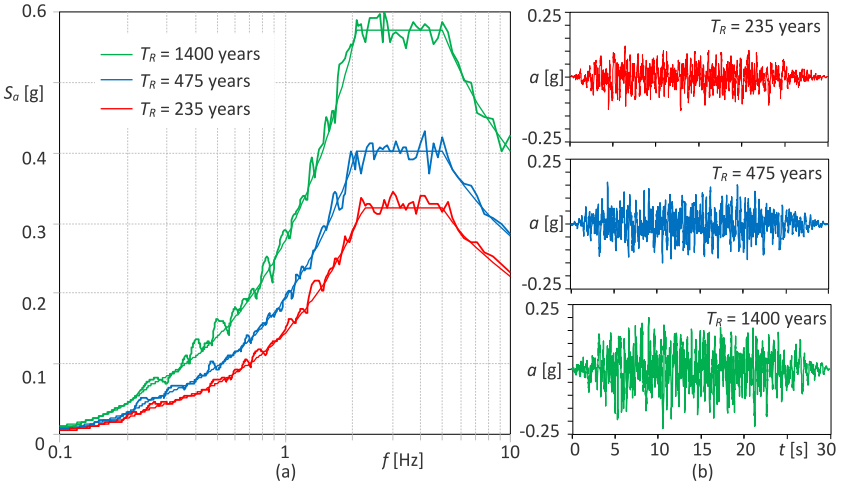

Fig. 2. (a) acceleration response spectra of the selected three seismic intensities; (b) artificial earthquakes adopted in the applications.

mean annual probability of occurrence approximated by the inverse of the return period of the event, the seismic hazard curve is constructed assuming a linear trend in the logarithmic plane between the seismic intensity measure and the mean annual probability of occurrence (European Committee for Standardization, 2005). The hazard curve has been adopted in this work to define seismic inputs of different intensity with the aim of investigating the response of the OWTs subjected to events of increasing importance. In detail, events characterized by return periods of 235, 475 and 1400 years have been considered, characterized by Peak Ground Accelerations (PGA) of 0.12, 0.16 and 0.23 g, respectively. It is worth noting that 475 years is the recurrence period of the ground acceleration indicated by IEC (2005)(art.11.6) for the seismic analysis of offshore wind turbines. In addition, according to European Committee for Standardization (2005), it corresponds to a probability of occurrence of 10% in 50 years, which is the one established by the code for performing seismic verifications at the life safety limit state. Finally, the return period of 1400 years corresponds to the ALE event for the selected seismic scenario. The response spectra associated to the three selected seismic intensities are shown in Fig. 2a.

Since the impact of earthquakes and the effects of soil–structure interaction on the dynamic response of the OWTs is investigated through nonlinear time history analyses, the seismic actions are represented through three artificial accelerograms matching each of the selected response spectra. Accelerograms have been obtained according to the Gasparini and Venmarcke (1976) spectrum-compatible nonstationary ground motion model and are shown in Fig. 2b. The duration of the seismic signals is 30 s in all cases. Finally, in Fig. 2a the 5% damped response spectra of the artificial earthquakes are compared with the reference ones.

2.3. Operating modes

In addition to the loads of seismic origin, the wind turbines will be assumed to be subjected to specific environmental loads while operating in three possible modes: power production, parked (standing still) and emergency shutdown triggered by the earthquake. In parked mode (PK), the generator is disconnected, rotor speed is set to zero and blade pitch angle is set to 90°. On the other hand, the structural response of the wind turbines will be studied considering two possibilities: (a) Power production (PP), in which the generator continues to run normally even when the earthquake arrives, and (b) Emergency shutdown (ES), in which an emergency stop is triggered when the first significant peak of the earthquake strikes the wind turbine. In that case, the generator is disconnected and the blades start to pitch at a rate of 8°/s in the NREL 5 MW turbine, and 2°/s in the IEA-10.0-198-RWT and IEA-15-240-RWT turbines. In all cases, turbines are subjected to category B (IEC, 2005) turbulent wind fields, generated using TurbSim (Jonkman, 2009), with a mean wind speed of 11.4 m/s at hub height, in each case, and assuming a Normal Turbulent Model (NTM, IEC, 2005) and a Kaimal spectral model. The submerged section of the support structure is also subjected to irregular wave loads, generated using the HydroDyn module through a JONSWAP/Pierson–Moskowitz spectrum incident wave kinematics model (Aranuvachapun, 1987) and adopting a significant wave height of the incident waves of 6 m, a peak-spectral period of the incident waves of 10 s, and full difference-frequency 2nd-order wave kinematics. Wind and waves are defined as acting aligned (co-directional) along the fore–aft direction. The self-weight of the structure is also taken into account at the beginning of the simulation. The gravitational loads of the members are computed within the SubDyn module and are later applied as appropriate forces and moments at the element nodes.

Table 4
Description of the whole set of cases analysed.

Wind turbine	Base condition	Operating mode	Earthquake	Direction of shaking	Time of arrival (s)
NREL 5 MW IEA-10-198-RWT IEA-15-240-RWT	FB CB	PP ES PK	$T_R = 1400$ years $T_R = 475$ years $T_R = 235$ years	FA SS	200 300 400
			No earthquake		

2.4. Set of cases for analysis

In order to understand the influence of the dynamic soil–structure interaction phenomena on the seismic response of the three offshore wind turbines described in Section 2.1, the support structures will be modelled considering the assumption of a simplified Fixed-Base (FB) at mudline, or a Compliant-Base (CB) model able to capture the dynamic response of the soil–foundation system corresponding to each turbine. To this end, frequency-dependent dynamic stiffness and damping functions of the monopile foundations in the different soil conditions are computed using the advanced boundary element–finite element model presented in Section 3.3 and then, this information is used to build a suitable LPM (see Section 3.4) able to represent efficiently the dynamic response of the soil–foundation system of each turbine in the framework of the nonlinear aero-hydro-servo-elastic simulation tool (see Section 3.2) used in this study. In all cases, the response of the turbines is simulated as operating in the three modes (PP, ES and PK) described in Section 2.3 when running in the absence of any seismic event, or when struck by any of the three earthquake signals described in Section 2.2 along the Fore–Aft (FA) or the Side-to-Side (SS) directions. On top of that, and given the irregular and variable nature of the environmental loads to which the system is subjected, the effect of the seismic actions is not independent of the time of arrival or the earthquake. For this reason, three different arrival times for the earthquakes (200, 300 and 400 s) are considered. This combination of parameters, summarized in Table 4, results in a total of 360 different simulations.

3. Methodology

3.1. Introduction

In this study, the dynamic response of the OWTs is simulated using the nonlinear aero-hydro-servo-elastic OpenFAST (OpenFAST Documentation, 2020) model in which the response of all the main elements (flexible blades, drivetrain, generator, control and electrical system, nacelle yaw, flexible tower, and support substructure), the environmental loads, and interaction phenomena such as aero-elastic and hydro-elastic interactions, are taken into account through specific models and modules. In order to be able to include also the dynamic properties of the soil–foundation subsystem and the ground input motion, the SubDyn module of the code has been modified, as described in Section 3.2. To characterize the soil–foundation subsystem, the dynamic response of the monopile foundation subsystem is computed though an advanced time-harmonic numerical model in which the monopile is discretized using shell finite elements and the surrounding soil is discretized using boundary elements, as described in Section 3.3. Based on the impedance functions computed from such model, suitable LPMs are built and introduced at the base of the wind turbine support structure (see Section 3.4), which allows taking into account the dynamic soil–structure interaction phenomena that influence the overall behaviour of the system, as shown later. Thus, the resulting coupled model for the turbine system takes into account, simultaneously, the material and radiation damping from the soil–foundation subsystem and the aero-elastic damping, both rigorously computed through the respective models, which allows a more accurate estimation of the dynamic response of the structure. This methodology allows to perform the parametric analysis described above in a sufficiently efficient way, and permits to focus on the main objectives of the present study.

3.2. Numerical model for the simulation of the seismic response of the offshore wind turbines

As said above, the numerical tool used in this study is based on OpenFAST, which is a numerical elasto-hydro-servo-elastic modular code for the simulation in time-domain of the response of land-based and offshore wind turbines. The code, mostly written in Fortran, is managed by a team at the National Renewable Energy Lab and is now an open-source project. The software is built using a framework in which the models that simulate different aspects of the system are programmed into modules that interact through a glue code that controls and coordinates the simulation, transferring data among modules at each time step. This glue code gathers all the information and drives the time-domain solution forward step-by-step using a predictor–corrector scheme. Time steps of $\Delta t = 0.0002$ s and $\Delta t = 0.0001$ s are set for fixed-base and compliant-base cases, respectively. This structure allows a multiphysics multifidelity approach to the problem, capacity to tackle different types of configurations and flexibility to introduce new subsystems and models.

In all the simulations presented in this study, the aerodynamic loads on blades and tower are computed using the AeroDyn module, which is able to take into account rotor wake and induction, blade airfoil aerodynamics, tower influence on the fluid local to the blade nodes, and tower drag; the structural dynamic responses of rotor, drivetrain, nacelle and tower are modelled using the ElastoDyn module, with a modal formulation for blades and tower, and a multi-body approach for drivetrain and nacelle; the control and electrical-drive dynamics are modelled using the ServoDyn module, simulating the control and electrical subsystems of the wind turbine; wave loads, and fluid–structure interaction phenomena are simulated using the HydroDyn module, in which a potential-flow theory solution, a strip-theory solution, or a combination of both, can be used for calculating the hydrodynamic loads on the submerged portion of the substructure; and the structural dynamic response of multimember fixed-bottom substructures, from the transition piece towards the base, is computed using the SubDyn module starting from a linear frame finite-element beam discretization of the structure. More details on the different modules can be found in OpenFAST Documentation (2020).

The SubDyn (Damiani et al., 2015) module was modified in order to be able to take into account dynamic soil–structure interaction and ground input motion. To this end, the equation of motion of the substructure is written as

$$\mathbf{M}\,\ddot{\mathbf{u}}^t(t) + \mathbf{C}\,\dot{\mathbf{u}}^t(t) + \mathbf{K}\,\mathbf{u}^t(t) = \mathbf{F}(t) + \mathbf{C}\mathbf{\Lambda}\,\dot{u}_b(t) + \mathbf{K}\mathbf{\Lambda}\,u_b(t) \tag{1}$$

where $\mathbf{M}$, $\mathbf{C}$ and $\mathbf{K}$ are the mass, damping and stiffness matrices including the terms corresponding to the LPM, as defined in Section 3.4, when a CB model is adopted, $\mathbf{F}(t)$ represents the external forces acting on the structure, $\mathbf{u}^t$ represents absolute displacements at the different degrees of freedom in the substructure, $u_b(t)$ is the input ground displacement at time t, the overdot denotes derivative with respect to time, and $\mathbf{\Lambda}$ is the influence vector representing the displacement of the different degrees of freedom as a consequence of the static application of a unit ground displacement (Chopra, 2017). Then, the beams in the substructure are modelled as Euler–Bernoulli or Timoshenko three-dimensional beams, and discretized using two-nodes 12-dofs finite elements defined by the stiffness and mass matrices presented in Damiani et al. (2015). The damping matrix for the substructure is built considering a Rayleigh Damping model (Chopra, 2017). The resulting equations of motion

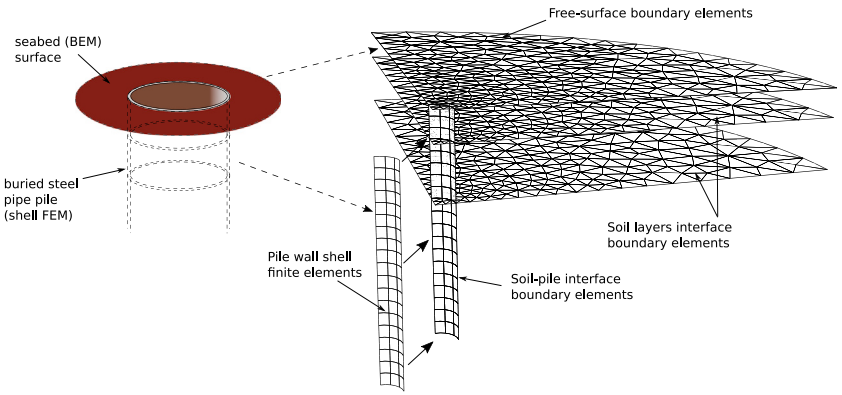

Fig. 3. BEM–FEM model of a monopile in a three layers soil and example of one of the meshes employed in the analyses.

must be cast in a form useful for implementation into the general framework of OpenFAST and SubDyn, taking into account the input variables to SubDyn and the output variables from SubDyn to other modules. To do so, the equations are written in state–space form, with one state system of equations, and two sets of output equations: one output equation to Elastodyn, in which the output variables are the interface forces at the transition piece between tower and substructure; and one output equation to HydroDyn, in which the output variables are absolute displacements, velocities and accelerations along the submerged elements of the substructure. This implementation of the input ground motion was verified for both fixed and compliant base conditions by comparison against results of an independent inverted pendulum finite-elements beam mode of the offshore wind turbine without incident wind or waves.

3.3. Numerical model for the computation of impedance functions

An advanced coupled model of boundary elements and finite elements (BEM–FEM model) previously developed in Bordón et al. (2017) is used to obtain the reference impedance functions of the monopile foundations described above. This model exploits the advantages of modelling the soil via boundary elements (Sommerfeld radiation condition implied and simple discretization) and the advantages of modelling the pile wall via shell finite elements (simple discretization and reduced number of degrees of freedom). An illustrative mesh for a given case (NREL 5 MW) is shown in Fig. 3.

The model is formulated in the frequency domain, where a circular frequency $\omega = 2\pi f$ is considered. The possibly layered soil has the following properties (one set for each layer): shear modulus G_s, Poisson's ratio ν_s, density ρ_s and hysteretic damping ratio ξ_s; where the complex effective shear modulus to be used is $G_s^* = G_s(1 + i2\xi_s)$. The use of the Boundary Element Method (BEM) allows the discretization of only the boundaries of each homogeneous region. The so-called Singular Boundary Integral Equation (SBIE) is used for collocating at the free-surface and the interfaces between soil layers:

$$\frac{1}{2}u_k^{\mathrm{i}} + \int_\Gamma t_{lk}^* u_k \,\mathrm{d}\Gamma = \int_\Gamma u_{lk}^* t_k \,\mathrm{d}\Gamma \tag{2}$$

where Γ is the boundary of the considered region, indices $l, k = 1, 2, 3$, and the Einstein summation convention is implied. The vector u_k^{i} is the displacement at the collocation point, u_k and t_k are the displacement and traction at the observation point, respectively, and u_{lk}^* and t_{lk}^* are the elastodynamic fundamental solutions in terms of displacements and tractions respectively. The so-called Dual (Singular and Hypersingular) BIEs are used for collocating at the interface between the soil and the shell mid-surface:

$$\frac{1}{2}\left(u_l^{\mathrm{i}+} + u_l^{\mathrm{i}-}\right) + \int_\Gamma t_{lk}^* u_k \,\mathrm{d}\Gamma = \int_\Gamma u_{lk}^* t_k \,\mathrm{d}\Gamma \tag{3}$$

$$\frac{1}{2}\left(t_l^{\mathrm{i}+} - t_l^{\mathrm{i}-}\right) + \int_\Gamma s_{lk}^* u_k \,\mathrm{d}\Gamma = \int_\Gamma d_{lk}^* t_k \,\mathrm{d}\Gamma \tag{4}$$

where $u_k^{\mathrm{i}+}, t_k^{\mathrm{i}+}$ and $u_k^{\mathrm{i}-}, t_k^{\mathrm{i}-}$ are displacements and tractions at the collocation point along the positive and negative shell mid-surface faces, respectively, and d_{lk}^* and s_{lk}^* are obtained from the differentiation of u_{lk}^* and t_{lk}^*. Standard triangular and quadrilateral quadratic boundary elements are considered for the discretization. On the other hand, shell finite elements based on the degeneration from the three-dimensional solid and free from the shear and membrane locking phenomena are considered. In particular, the element used is the MITC9 element which uses the Mixed Interpolation of Tensorial Components (MITC) methodology to the standard quadratic shell finite element (Bucalem and Bathe, 1993). Finally, a conforming mesh between the soil-shell interface and the shell mid-surface is considered, and the coupling is performed by imposing welded conditions through compatibility and equilibrium conditions. Herein, the soil is modelled as a viscoelastic medium, although the numerical framework allows the consideration of Biot's poroelastic models for the soil. The model is presented in detail, and validated, in Bordón et al. (2017) and Bordón (2017).

3.4. Lumped parameter model

Dynamic soil–structure interaction is introduced in the offshore wind turbine model through an LPM at mudline level that represents the dynamic response of the foundation–soil subsystem. Among the different LPMs existent for this type of problems, an efficient model in accordance with the nature and the reduced complexity of the impedance functions computed for this problem has been selected. Thus, the LPM employed in this work, is the one originally proposed and validated by Carbonari et al. (2018), and later used and tested, for instance, in González et al. (2019) and Morici et al. (2019), and depicted in Fig. 4a. The coupled roto-translational behaviour is represented through a two-degree-of-freedom system per horizontal plane (xz and yz planes), each with a translational mass m_h and a mass moment of inertia I_r at the interface between the underground section of the foundation and the substructure above mudline, connected to the soil through the corresponding translational and rotational pairs of constant springs and dashpots k_h, c_h, k_r, and c_r and, at the same time, connected to an additional eccentric translational mass m_t through a rigid massless link of length h_1 that is connected to the soil through additional spring and dashpots k_t and c_t at distances h_3 and h_2, respectively. The LPM configuration, characterized by eccentric elements, allows to model and fit simultaneously the translational, rotational and horizontal-rocking coupled impedance functions with important advantages in this type of applications. On the other hand, the vertical and torsional impedances, more regular and with less influence on the response of the turbines, are modelled using first-order LPMs, as depicted in Fig. 4b. In all cases, the values of the parameters of the LPMs are found through a non-linear least squares fitting procedure, as described, for instance, in González et al. (2019). The resulting LPM is introduced in the finite elements model of the substructure as an additional element at mudline level.

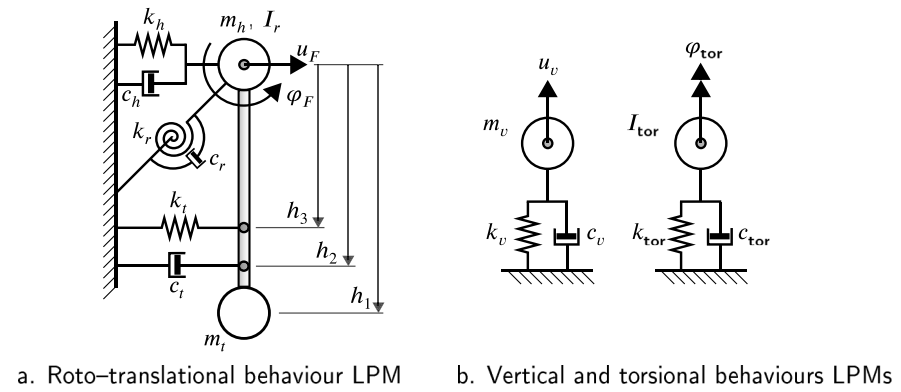

Fig. 4. Scheme of the LPM adopted for lateral vibrations (a) and of the mass–spring–damper models, adopted for vertical and torsional vibrations (b).

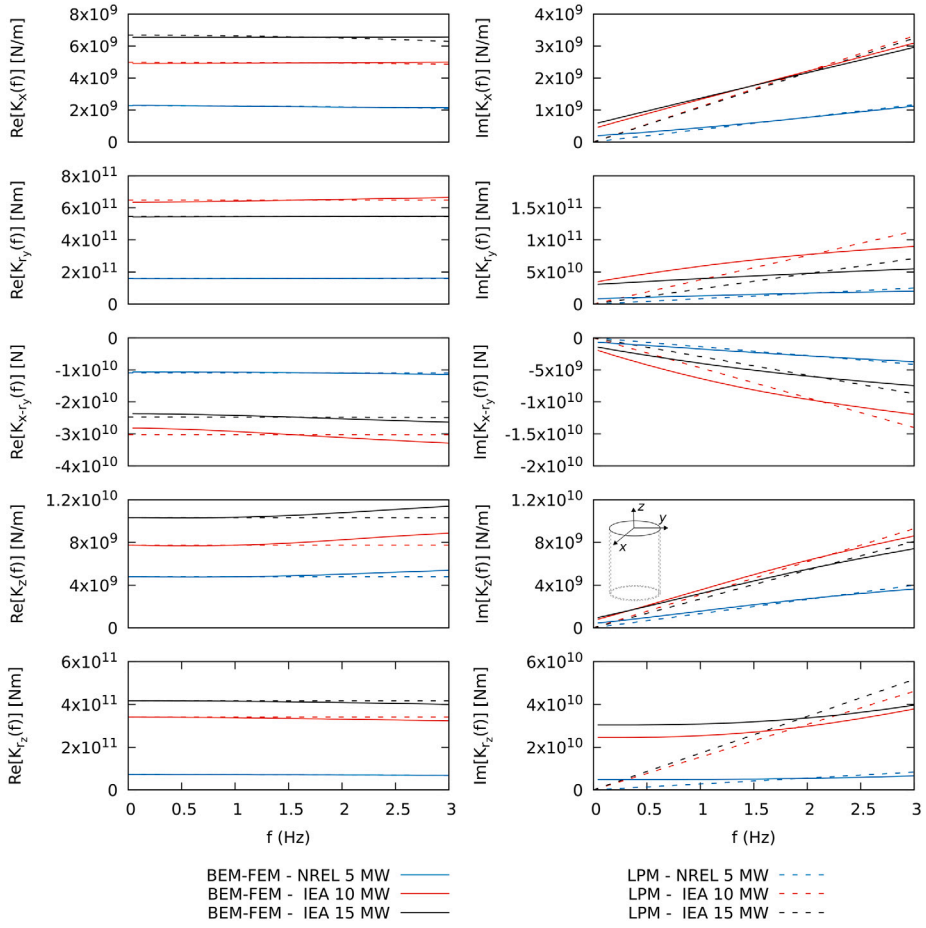

Fig. 5. Real and imaginary parts of the translational, rotational, crossed-coupled horizontal-rocking, vertical and torsional impedance functions obtained from the BEM–FEM model and provided by the fitted LPMs for the three soil–foundation cases.

4. Results and discussions

4.1. Impedance functions

The impedance functions computed for the monopile foundations of the three different offshore wind turbines are presented in Fig. 5. Real and imaginary parts of the translational (K_x), rotational (K_{r_y}), crossed-coupled horizontal-rocking (K_{x-r_y}), vertical (K_z) and torsional (K_{r_z}) impedance functions obtained from the BEM–FEM model described in Section 3.3 are plotted as a function of frequency. The time-harmonic stiffness and damping functions provided by the fitted Lumped Parameter Models built for each case are also presented in dashed lines in the same figure. It is worth noting that the monopile foundation corresponding to the IEA-15-240-RWT is the translationally, torsionally and vertically stiffest of the three, while the foundation of the IEA-10-198-RWT is rotationally slightly stiffer due to its significantly greater

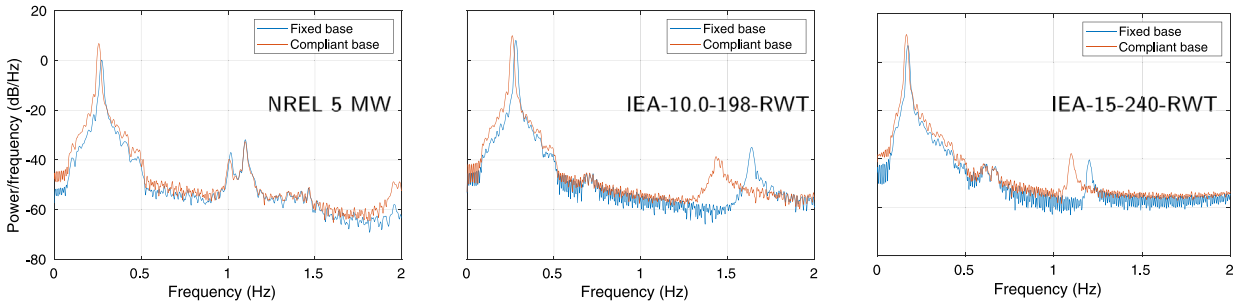

Fig. 6. Power Spectral Densities in the fore–aft direction obtained from the response of the 5, 10 and 15 MW turbines (left to right) in parked conditions, under fixed and compliant base hypotheses.

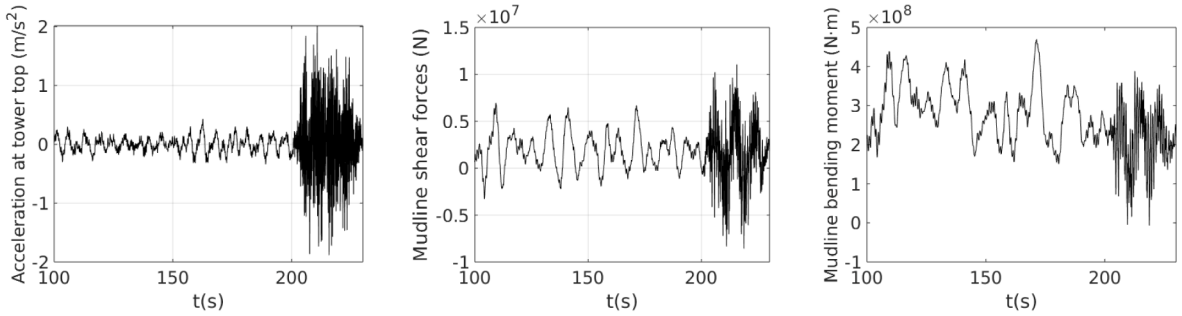

Fig. 7. Time history responses corresponding to accelerations at the tower top, pile shear forces at mudline and pile bending moments at mudline for the 15 MW OWT subjected to seismic excitation at $t = 200$ s in the fore–aft direction in power production mode.

thickness. The errors obtained when comparing the static stiffnesses provided by the reference BEM-FEM solution and by the fitted Lumped Parameter Model are always below 2.1%, with the only exception of the crossed-coupled case, in which the error reaches 7.5% for the IEA-10-198-RWT case. The worst fitting is achieved in the case of the damping terms in the low frequency range, especially in the torsional impedance. Overall, the calibrated LPMs are able to reproduce well the frequency dependent behaviour of the foundation impedances in the frequency range in which the resonance frequencies of the turbines fall.

4.2. Frequency response

Fig. 6 presents the FA Power Spectral Densities of the three offshore wind turbines, respectively, obtained from the FA accelerations at the tower top under parked conditions subjected to environmental loads, from which natural frequencies are most clearly obtained. The 430 s of simulation are used in all cases. Each plot presents the spectra considering fixed base and also compliant base hypotheses, from which the effect of SSI is clearly observed. The second natural frequency is hardly affected by SSI in the case of the 5 MW turbine, but significantly affected in the cases of 10 and 15 MW cases. Table 5 presents the fundamental frequencies for the three wind turbines, computed from these spectra, also in the side-to-side direction. For each turbine, the period lengthening in the FA and SS directions is similar, with mean values around 6%, 8% and 5% for the 5, 10 and 15 MW turbines, respectively. It is worth noting that the long fundamental periods of the structures under study, around 4 s in the case of the 5 and 10 MW turbines and around 6 s in the case of the 15 MW, are the main reason why the design of large wind turbines is generally not expected to be dominated by seismic actions, considering that for long fundamental periods of vibration, spectral amplitudes of the earthquakes are moderate or low (Katsanos et al., 2016; Bhattacharya and Goda, 2016).

4.3. Seismic response

4.3.1. Time history structural response

In order to illustrate how the systems behave under the seismic actions described in Section 2.2, Fig. 7 presents the example of the time histories of the FA accelerations at the tower top, pile shear forces at mudline in the FA direction, and the pile bending moments at mudline around the SS direction of the IEA-15-240-RWT in power production mode when subjected to the seismic input acting in the FA direction and defined for a return period of 1400 years (PGA = 0.23 g) at $t = 200$ s into the simulation. The first 100 s of simulations are always discarded, after which the solution has always already converged to the stationary operational response of the system. These first 100 s of simulations will neither be taken into account when analysing the results in the following sections. The plots allow to observe the magnitudes and characteristics of the structural response of the turbine when operating under nominal conditions subject to loads from wind and sea, and how they are affected by the arrival of the seismic event. It also allows to understand why the response under earthquake loads will depend on the specific time at which the seismic signal strikes the system. The following sections are aimed at synthesizing the large amount of results obtained in order to be able to draw general conclusions.

4.3.2. Peak seismic response

Fig. 8 shows the peak accelerations along the FA direction obtained at the top of the OWT towers when the earthquake input acts in the FA direction, together with the peak shear forces (in the FA direction) and bending moments (around the SS direction) at the pile cross-sections at mudline. Similarly, Fig. 9 shows the tower top peak accelerations in the SS direction when the earthquake input acts in the SS direction, together with the pile peak shear forces and bending moments at mudline in the SS direction and around the FA direction, respectively. Peaks are always computed as absolute maxima (i.e. regardless of the sign). In each plot, results are presented in six columns of markers, with the first three columns referring to FB models in PP, PK and ES modes, and

Table 5
Fundamental frequencies obtained for Fixed Base and Compliant base conditions.

	NREL 5 MW	IEA-10.0-198-RWT	IEA-15-240-RWT
Fixed base, fore–aft:	0.272 Hz (3.68 s)	0.281 Hz (3.56 s)	0.172 Hz (5.81 s)
Compliant base, fore–aft	0.256 Hz (3.91 s)	0.261 Hz (3.83 s)	0.164 Hz (6.10 s)
Fixed base, side-to-side:	0.273 Hz (3.66 s)	0.280 Hz (3.57 s)	0.172 Hz (5.81 s)
Compliant base, side-to-side	0.260 Hz (3.85 s)	0.259 Hz (3.86 s)	0.164 Hz (6.10 s)

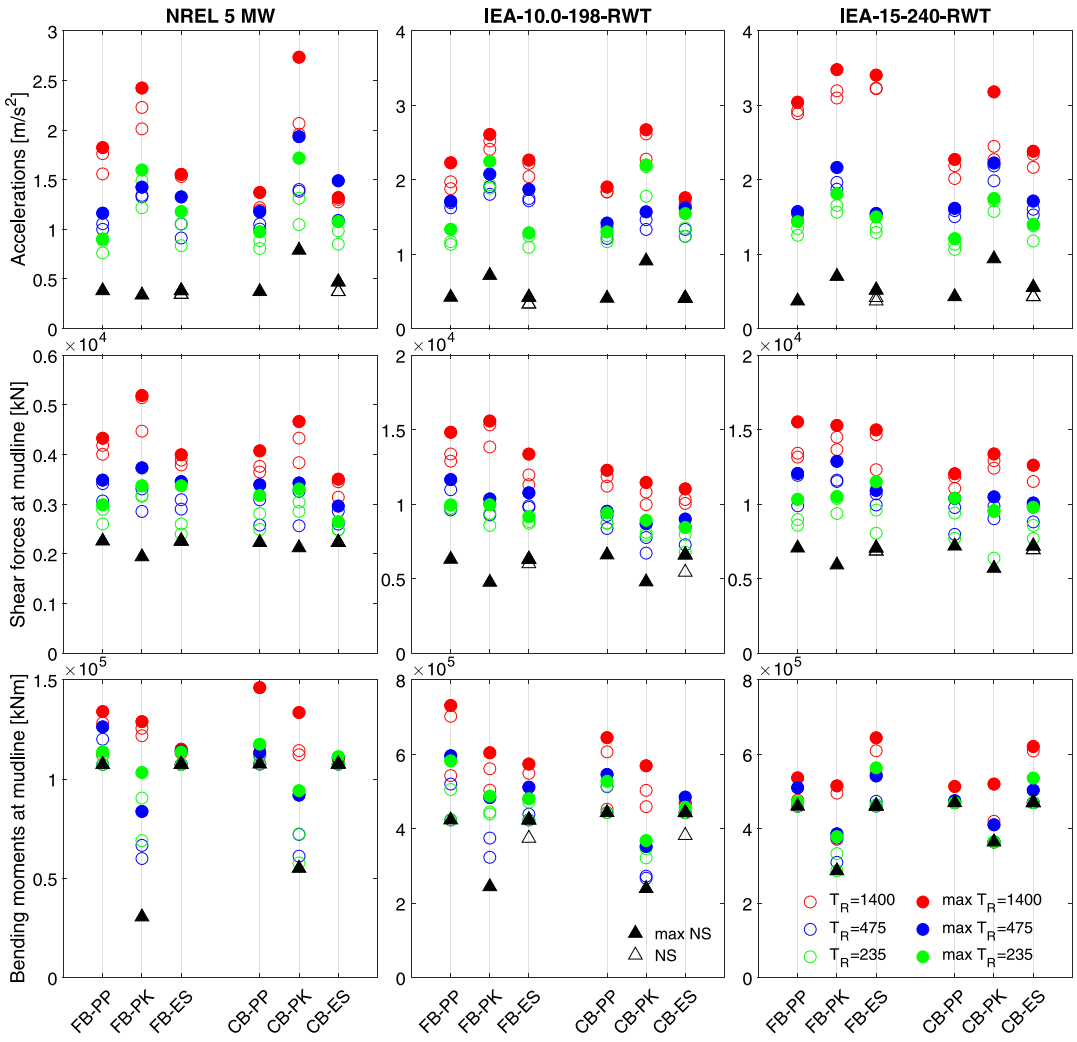

Fig. 8. Peak responses in terms of accelerations at the tower top, pile shear forces at mudline and pile bending moments at mudline for all situations and OWTs. Fore-aft response.

the other three columns to CB models in PP, PK and ES modes. Colours are used to distinguish between the three seismic intensities, and the magnitude of the peak responses for each individual time of arrival is represented with a circle, with filled coloured circles used to indicate the maximum value among these three arrival times. Triangles are used to report the magnitude of the peak responses when the systems are not subject to any seismic event (NS); in this case, a single analysis is performed for each case in PP and PK modes, while three analyses are run for each case in the ES mode, by supposing a stop of the turbines in absence of seismic actions at different times, corresponding to the three arrival times assumed for the earthquakes. This will make possible a direct comparison of the system responses under normal conditions (NS) and under seismic excitation. Each column of plots in Figs. 8 and 9 refers to a specific OWT, and each row of plots to a response quantity.

The increase in peak responses induced by the seismic actions is very relevant in most cases and response quantities, although mudline bending moments in the FA direction are less affected due to the already large effect of the environmental loads in such a case. At the same time, soil–structure interaction often plays a beneficial role in the FA direction, with exceptions in the case of the NREL 5 MW turbine, while in the SS direction, SSI is generally beneficial for the IEA-10-198-RWT and IEA-15-240-RWT, and detrimental for the NREL 5 MW turbine. The difference between seismic demands computed for the same seismic signal at different arrival times is, in some cases, quite relevant, mainly in the FA direction (because the effects of the environmental loads, highly time-dependent, are more relevant in this direction) but also in the SS direction. Of course, the magnitude of the

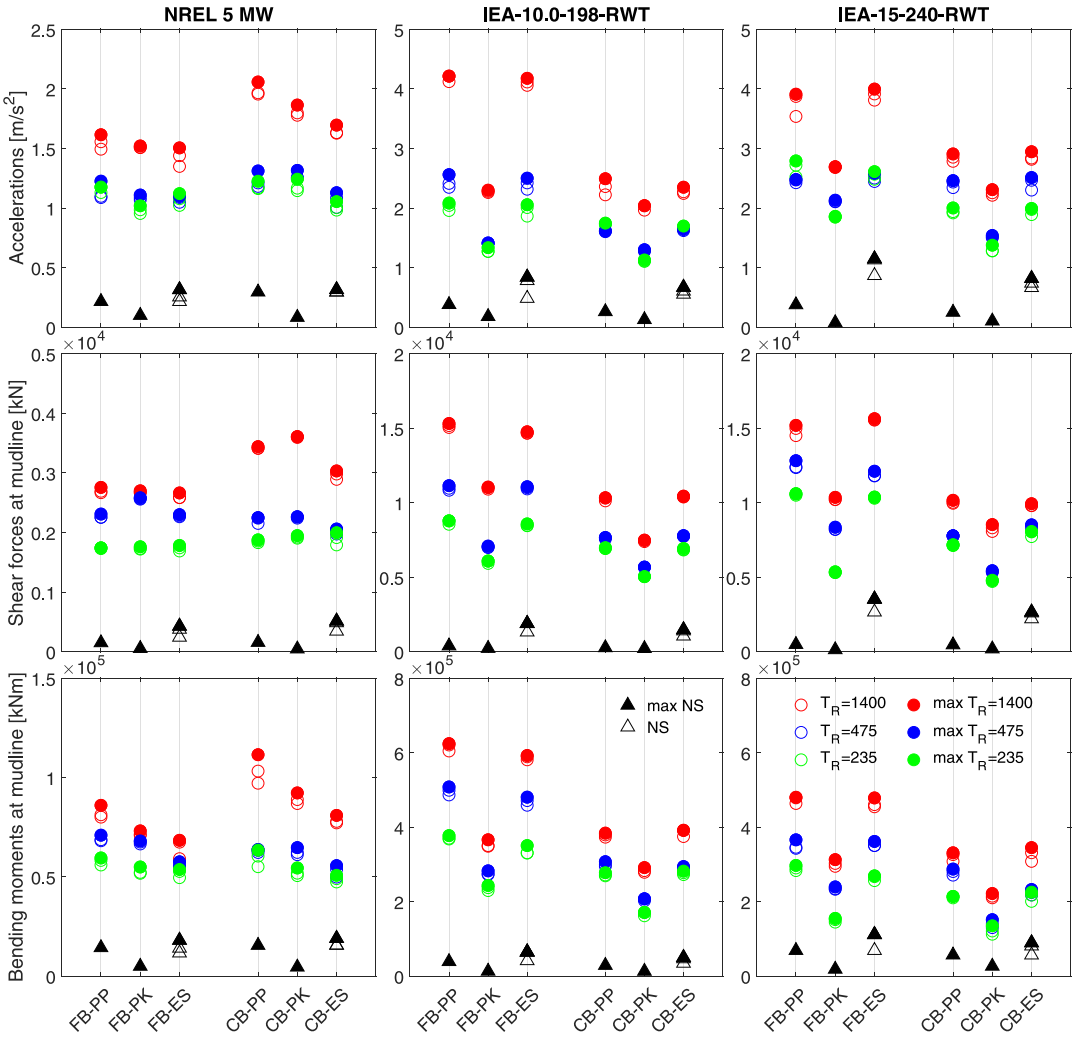

Fig. 9. Peak responses in terms of accelerations at the tower top, pile shear forces at mudline and pile bending moments at mudline for all situations and OWTs. Side-to-side response.

seismic response depends strongly on the intensity of the earthquake input, although larger seismic demands can be obtained for less intense earthquake inputs for some cases, depending on arrival times and the rest of characteristics of the systems.

The peak values of the three response quantities analysed (tower top accelerations, and pile shear and bending moments at mudline) obtained for the IEA-10-198-RWT and IEA-15-240-RWT systems are larger than those computed in the case of the NREL 5 MW turbine, being this increase especially significant, as expected, in the case of mudline bending moments and shear forces (with an increase by a factor of around 5–6), and less significant in the case of tower top accelerations (with an increase by a factor of around 1.5–2, despite the differences in geometries, structural characteristics, mass and inertia, and properties of foundation and soil). The peak responses registered for the IEA-10-198-RWT and IEA-15-240-RWT systems are of comparable magnitudes. Thus, there is not a progressive trend of increasing demands for increasing size. In this regard, it is worth highlighting that, for the specific turbines analysed in this study, the fundamental frequencies do not follow a progressive trend neither, with the IEA-10-198-RWT showing a fundamental frequency very similar to that of the NREL 5 MW OWT (see Table 5) due to the significant stiffness the support structure of the former (see Table 1). Thus, the same observation about the absence of a clear progressive trend can be made for the spectral accelerations corresponding to the system fundamental frequency for a common damping ratio. However, the damping ratio is not constant for both structures or for different cases, as it depends on aerodynamic damping. Aerodynamic damping, due to the aeroelastic interaction between blades and air, plays a very significant role in the overall structural damping ratio of the wind turbine. This aerodynamic damping depends, for instance, on rotor speed, rotor size and wind (see Valamanesh and Myers, 2014 or Meng et al., 2020) and will, therefore, be different for both turbines, affecting differently the seismic response of each one of the systems.

Peak accelerations in the FA direction tend to be larger when the turbine is parked because, in this operating mode, the amount of aerodynamic damping from aeroelastic interaction is much smaller (Meng et al., 2020; Kitahara and Ishihara, 2020). For the same reason, the magnitudes of the peak accelerations in the SS direction for the IEA-10-198-RWT and IEA-15-240-RWT systems tend to be larger than in the FA direction for the PP and ES modes, but lower in PK mode due to the angle of the blades in such mode of operation. The magnitude of these effects differs from turbine to turbine, and is a very relevant aspect

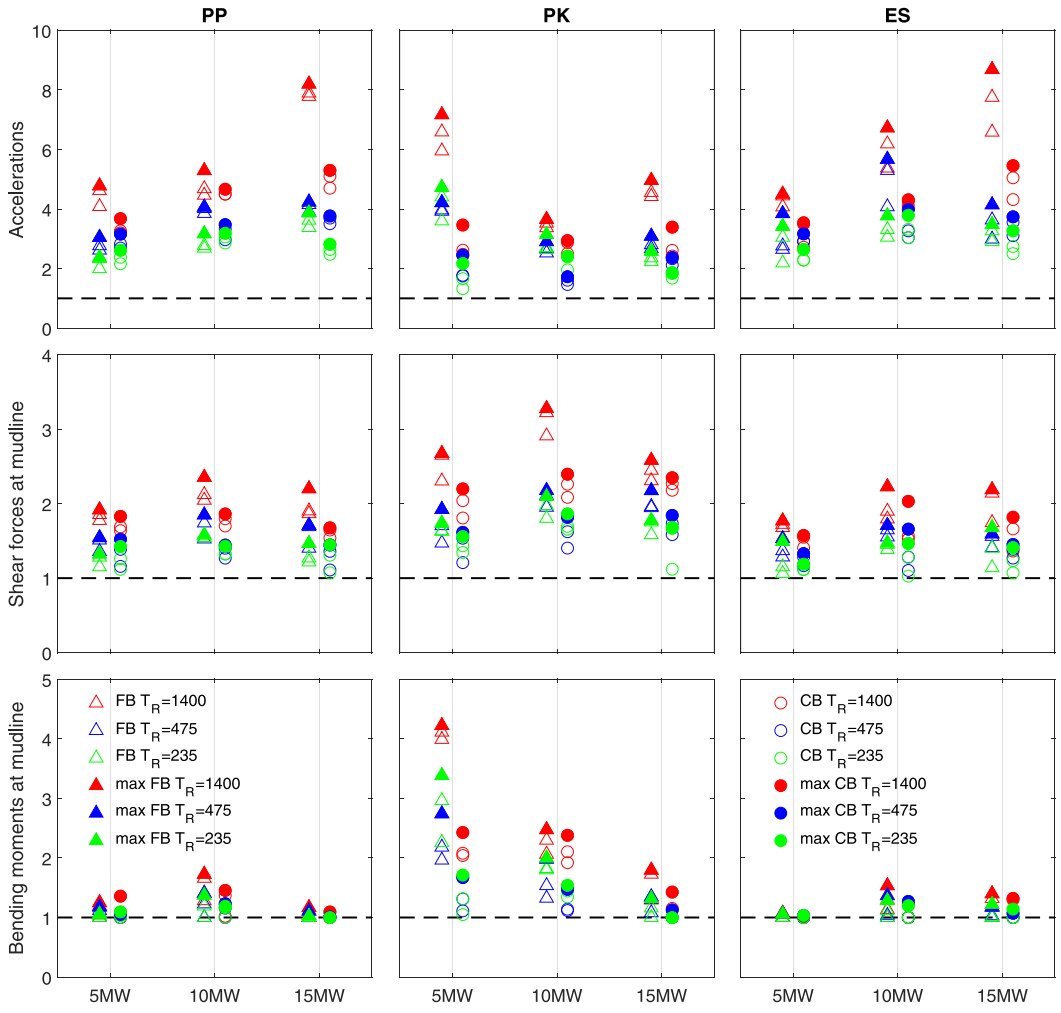

Fig. 10. Ratios between peak seismic responses and peak non-seismic response of accelerations at the tower top, pile shear forces and bending moments at mudline. Fore-Aft response.

that is not easily captured by simplified models in which aeroelastic interaction is not modelled in detail.

In order to quantify the impact of the seismic excitation on the response of the OWTs, the peak accelerations at the tower top, and the peak shear forces and bending moments at the mudline computed under seismic action are normalized with respect to the peak accelerations at the tower top, and the peak shear forces and bending moments at the mudline, respectively, obtained in the NS condition. These ratios are shown in Figs. 10 and 11 for the FA and the SS directions, respectively. In this case, each column of plots refers to a specific mode of operation, while each row of plots corresponds to a response quantity. Each plot contains the results corresponding to the three turbines, and the ratios relevant to FB and CB conditions for each turbine are plotted separately along two different verticals with triangles for FB and, alongside, circles for CB. Again, colours are used to distinguish between the three seismic intensities. Empty symbols are used to present results obtained for the three seismic intensities and arrival times of the earthquakes while filled symbols indicate the maximum values of the ratios. A reference horizontal dashed line is included in all plots to distinguish easily between ratios above or below unity.

From an overall point of view, the magnitude of the three response quantities under study experience a significant increase as a consequence of the seismic actions. In the FA direction, accelerations present the highest ratios and reveal to be the most sensitive response quantity to earthquakes: increments ranging from about 100 to 700% are found, depending on the seismic intensity, the OWT and the operating mode. Increments in shear forces and bending moments are less pronounced. Shear forces experience increase by factors of up to 3 under the FB assumption, and up to 2.4 times under the CB hypothesis, which predicts smaller efforts in almost all situations. Bending moments show less relevant increases, with the only exception of the PK condition, not because the seismic response is higher, but because the reference NS bending moment is significantly smaller (see Fig. 8).

As previously observed, increments of the response quantities with respect to the NS condition are much more pronounced in the SS direction (Fig. 11). However, it should be remarked that this phenomenon is not due to a greater seismic response of the OWTs in the SS direction but rather to a minor demand in the SS direction due to NS loads. Indeed, the seismic demand is not so dissimilar between directions, as seen when comparing Figs. 8 and 9. It is worth observing that the seismic actions govern the response in the SS direction, producing accelerations from 5 to more than 20 times higher than those computed for the NS condition, with a peak ratio above 35 times the NS response for the 15 MW turbine on FB. Similarly, shear forces and bending moments at the mudline pile cross sections are largely dominated by earthquakes. The less important increments are registered for the ES operating mode for which the peak values of accelerations at the tower

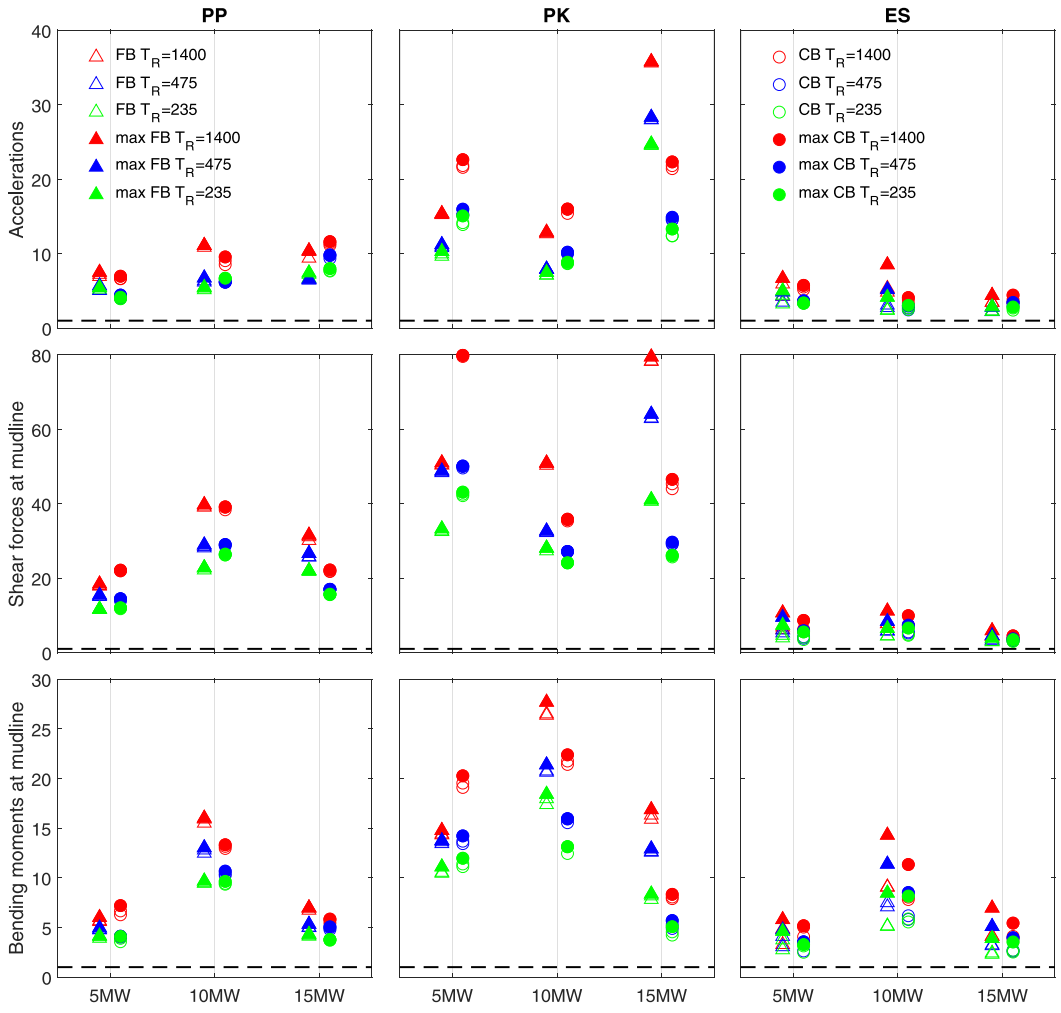

Fig. 11. Ratios between peak seismic responses and peak non-seismic response of accelerations at the tower top, pile shear forces and bending moments at mudline. Side-to-side response.

top are up to 10 times higher than those at NS condition, and for which peak shear forces and bending moments are about 10 and 5 times higher, respectively, with the only exception of bending moments relevant to the 10 MW turbine. This is clearly due to the fact that the ES of the turbine, in absence of earthquake, triggers an important response of the turbine in the SS direction.

4.3.3. *Influence of dynamic soil–structure interaction*

The role of SSI on the seismic and NS response of the investigated OWTs is analysed by normalizing the peak response quantities obtained from the CB systems with the relevant ones obtained from the FB models. Figs. 12 and 13 show these ratios for the FA and SS directions, respectively. Each column of plots within the figures refers to a specific mode of operation, while each row of plots corresponds to a response quantity. Again, colours are used to distinguish between the three seismic intensities, and two sets of results are presented for each OWT in slightly separated vertical lines: the left one corresponding to non-seismic response, and the right one corresponding to seismic response. Empty symbols are used to present each individual ratio, while filled symbols indicate the maximum values of these ratios when relevant. For the NS situation, a set of three ratios is presented for the ES operating mode, by supposing the emergency stop of the turbine in absence of earthquake at three different times, corresponding to the arrival times of the earthquakes. Black horizontal dashed lines are used to separate portions of the plots in which the SSI is detrimental (ratios greater than 1), or beneficial (ratios lower than 1) to the structural response.

In the FA direction, effects of SSI are moderate in absence of earthquake excitation, with the exception of the PK operating mode and the accelerations for the ES operating mode, and showing, in most cases, a detrimental effect of SSI. A significant increase in both peak accelerations and bending moments due to SSI is observed under NS loading for the PK operating mode of the 5 MW and the 15 MW turbines in line with the increase in peak power spectral density observed in Fig. 6, obtained also in PK conditions. Under seismic excitation, on the contrary, SSI tends to be beneficial to the structural response although ratios greater than one can be observed, especially for the PK operating mode. Even if a general trend is difficult to outline, there is a significant number of situations in which the beneficial effects are more relevant for increasing intensities of the seismic excitation: for example, the highest ratios of shear forces relevant to events with return periods of 475 and 1400 years are all below one, with ratios relevant to events with a return period of 1400 years very often below ratios of events with a return period of 475 years. Similarly, the highest ratios of bending moments relevant to the event with 1400 year return period are near or below one, and often lower than ratios relevant to earthquakes with lower intensities.

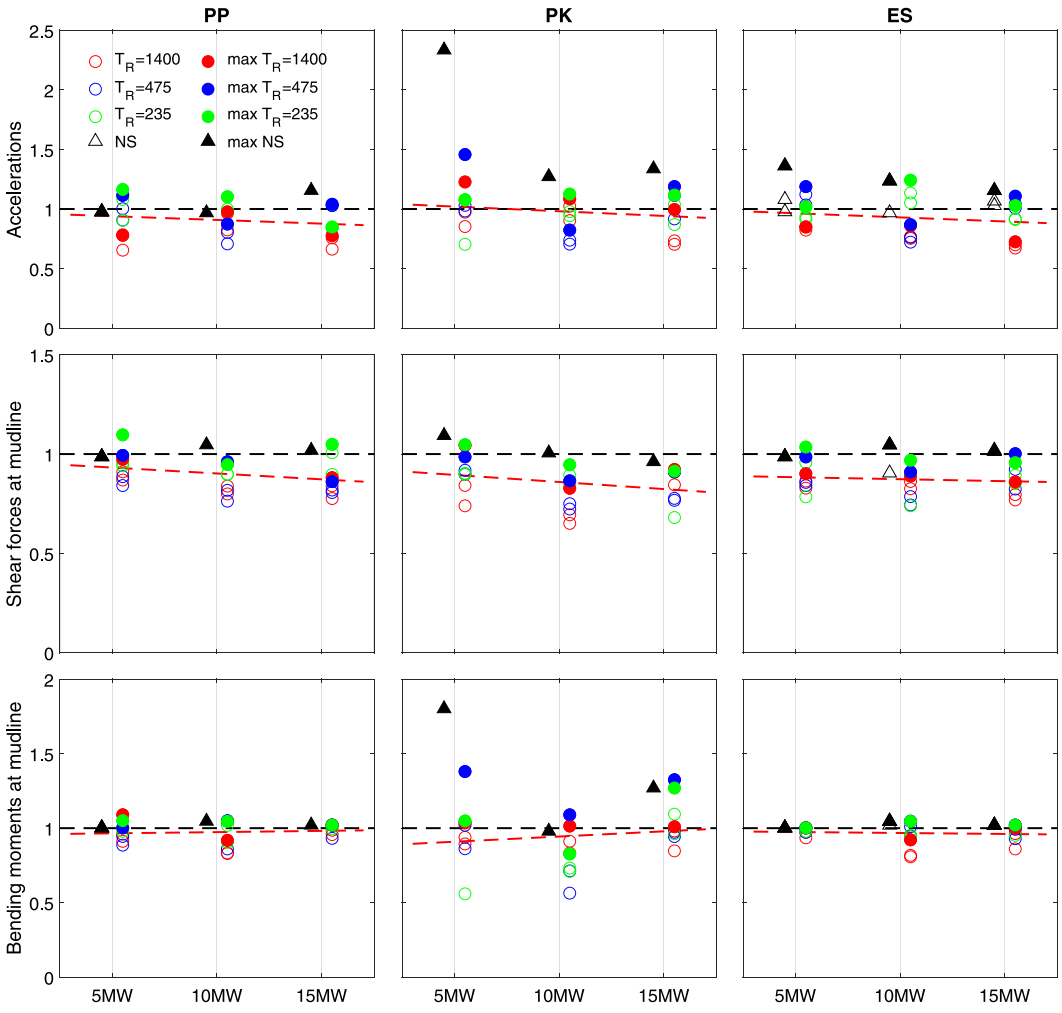

Fig. 12. Ratios between peak seismic and non-seismic responses computed under the CB assumption and those obtained under a FB hypothesis. Fore-Aft response.

Regarding the effects of SSI in the SS direction (Fig. 13), SSI can now produce beneficial or detrimental effects depending on the case, and also under NS loading, but a clear trend with rated power is seen, with a clear increase in the benefits of SSI when the size of the OWT increases. In order to highlight more clearly such a trend, a red dashed tendency line (obtained by fitting through least-squares on the rations corresponding to the seismic response of all turbines in each case) has been also included in the plots. In the SS direction, it is very clear that the larger the turbine, the more significant are the beneficial effects from SSI. This trend can also be observed in the FA direction, although its effects are generally much less clear.

With the aim of condensing further this information, Fig. 14 illustrates the influence of SSI by plotting peak accelerations, peak mudline shear forces and peak mudline bending moments, computed for the different OWTs under seismic excitation, together with the maximum ratios of such magnitudes with respect to the same variable under NS loading. Note that each plot presents, for every case, the maximum values of these ratios and variables among the three earthquakes and times of arrival. At the same time, each web presents a symmetry because the right and left of the same horizontal present maximum peak values and maximum ratios of the same magnitude, respectively. At the same time, the upper third of each plot corresponds to accelerations, while the centre represents mudline shear forces and the lower third corresponds to mudline bending moments. In all cases, the numerical values of the ticks in the axes has been omitted for simplicity, but the first subdivision of every radii corresponds always to zero, while the axes limits are the same in all web plots of the same figure, to allow for visual comparison. The maximum value of each radius corresponds always to the maximum value for that axis in all the plots of the figure, so axes can be understood as normalized between 0 and 1. In this figure, the three rows present results for the three turbines while the three columns present results for the three operational modes. It is quite clear that SSI is generally beneficial (blue line, corresponding to the fixed base case, acts as an envelope of the rest of curves in virtually all situations). Again, a clear trend with rated power is observed, with larger effect of SSI for larger OWTs.

4.3.4. *Influence of mode of operation*

Finally, in order to look into the influence of the mode of operation on the seismic behaviour of the OWTs, Fig. 15 gathers those peak accelerations, peak mudline shear forces and peak mudline bending moments, computed for the different OWTs under seismic excitation, together with the maximum ratios of such magnitudes with respect to the same variable under NS loading, in a figure arranged similarly to the previous case, but corresponding the rows in this case to the base models (Fixed base or Compliant Base) and the columns to the three turbines. Now, each web plot is built with three lines, one per operating mode.

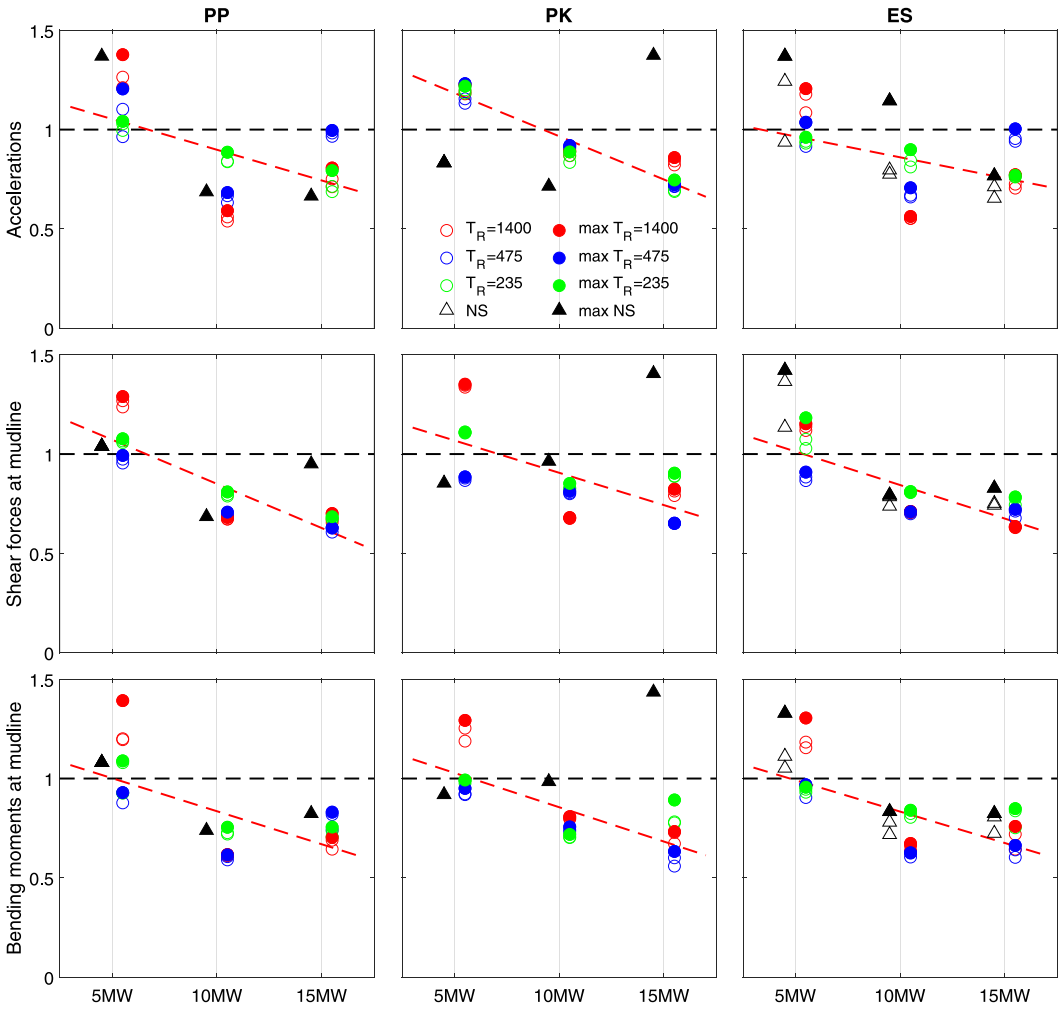

Fig. 13. Ratios between peak seismic and non-seismic responses computed under the CB assumption and those obtained under a FB hypothesis. Side-to-side response.

The conclusion depends on the turbine. In the case of the 5 MW turbine, the emergency shutdown operation mode is clearly beneficial (yellow line tends to be an internal envelope). For the other two cases, the ES operating mode tends to produce the smaller increases in response with respect to the NS loading condition but, at the same time, can produce the largest seismic demand in the case of the 15 MW turbine, being on the contrary, the PP operating mode the one that produces the highest seismic demand in the case of the 10 MW OWT. Of course, the parameters of the ES can be quite different to those assumed in this study, which could lead to different observations in this regard.

5. Conclusions

This paper has summarized the main results of a study on the response of three large offshore wind turbines, with rated powers of 5, 10 and 15 MW, to low or moderate intensity earthquakes, and taking soil–structure interaction into account. To do so, an aero-hydro-servo-elastic model of the different turbines have been taken into account, and the dynamic response of the different monopile foundations have been modelled using an LPM fitted to the results of an advanced linear time – harmonic boundary element – finite element model. Thus, the energy dissipated through the soil–foundation system and through aeroelastic damping are simultaneously taken into account directly by the model. The study has taken into account also the environmental loads and aspects such as the possibility of different times of arrival of the earthquake input.

It has been found that even low or moderate intensity earthquakes as the ones simulated in this study can produce significant increases in the structural demands of the offshore wind turbines in terms of accelerations at the top of the towers and of bending moments and shear forces at mudline, with bending moments in the fore–aft direction experiencing the less pronounced increases because, in this case, the efforts associated to the seismic response are added on top of the already important bending moments associated to resisting the thrust from the rotor. It is for this reason that the maximum bending moments appear always for Power Production or Emergency Shutdown operating modes, but even so, differences among earthquakes are very significant (also in Power Production) which reveals the relevance of the seismic actions. The increase of accelerations at the tower top, where the nacelle is located, should be carefully considered in the design of the anchoring systems of the nacelle components to the structure itself (e.g. gearbox, generator, brakes) because of the increase of inertia forces to which they are subjected. Similarly, seismic actions may be crucial for the pile design, which is subjected to sensibly higher stress resultants during earthquakes than those due to loads at service conditions.

The magnitude of the increase observed in all variables depends on each specific case, and varies for different operating modes, turbine

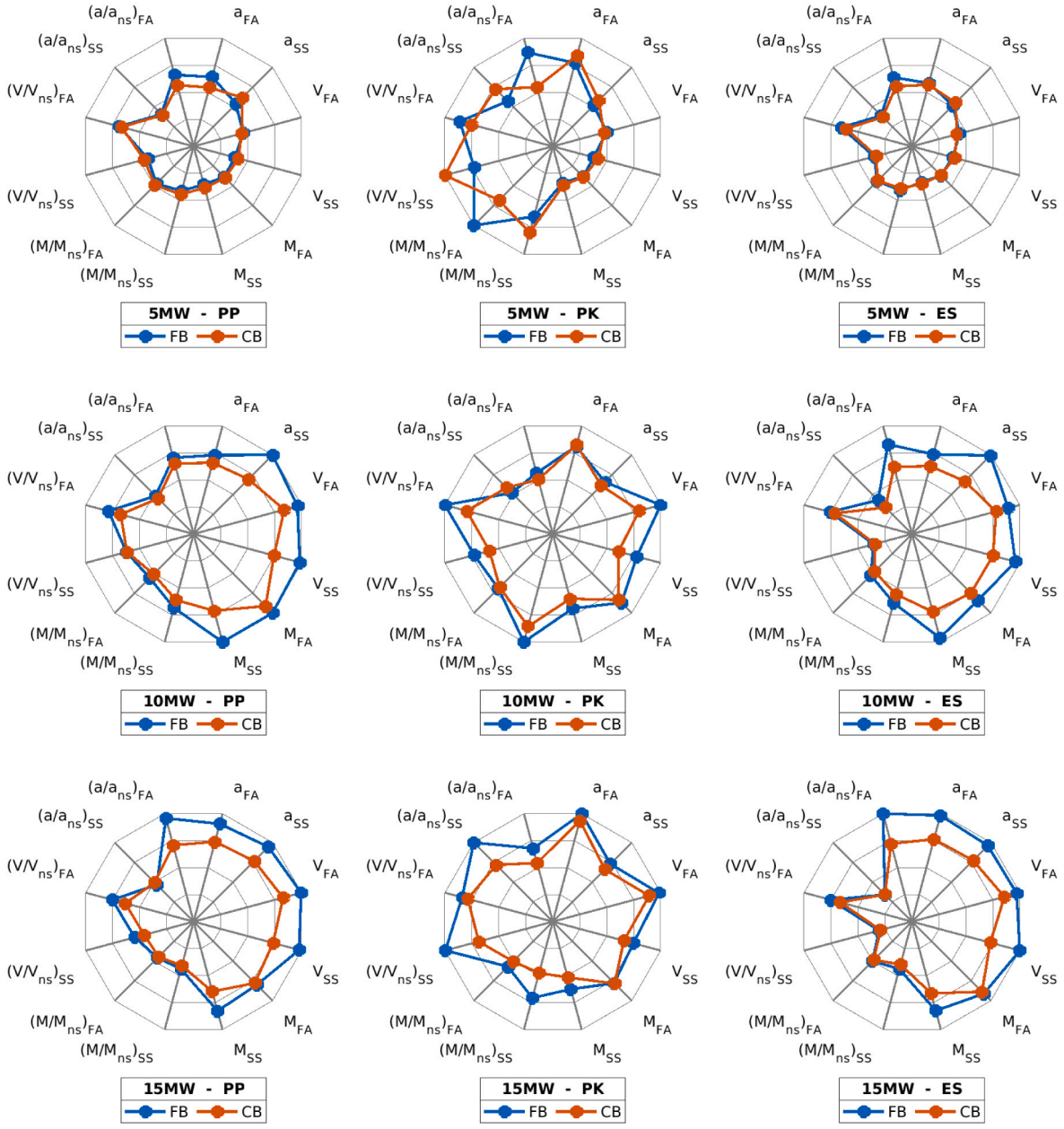

Fig. 14. Influence of SSI on the response of the OWTs. (a = Acceleration; M = Mudline Moment; V = Mudline shear force; NS = Absence of seismic input). The first subdivision of every radii is always 0. The axes limits is the same in all web plots in this figure to allow comparison. (For interpretation of the references to colour in this figure legend, the reader is referred to the web version of this article.)

rated powers and modelling assumptions for the foundation. In this regard, dynamic soil–structure interaction has been found to play a significant role. It can be beneficial or detrimental to the structural response, depending on the case, but it has been found that there exists a clear tendency for dynamic soil–structure interaction to be beneficial when the size of the offshore wind turbine increases, being this tendency very strong in the side-to-side direction. At the same time, in the fore–aft direction, the effects of soil–structure interaction are moderate in the absence of earthquake excitation and are, in most cases, detrimental. Under seismic excitation, on the contrary, dynamic soil–structure interaction tends to be beneficial to the structural response. It can be concluded that the soil–foundation compliance should be considered in projects located in zones with seismic risk in order to be able to compute a reliable prediction of the structural response. The influence of other aspects such as arrival times of the earthquake is also worth being taken into account.

The best strategy to follow in order to reduce the impact of the earthquake on the structural demand of large offshore wind turbines should be carefully evaluated in each case. Indeed, aspects such as the superposition of effects must be taken into account, and aeroelastic damping could play a very beneficial role in many cases. It is not clear, a priori, whether triggering an emergency stop under the arrival of an earthquake, or continuing on power production, if possible, is better from an structural point of view. Of course, the parameters of the emergency shutdown can be quite different to those assumed in this study, which could lead to different conclusions in this regard. Also, this parametric analysis has been performed considering a linear model for the soil–foundation subsystem which allowed to investigate

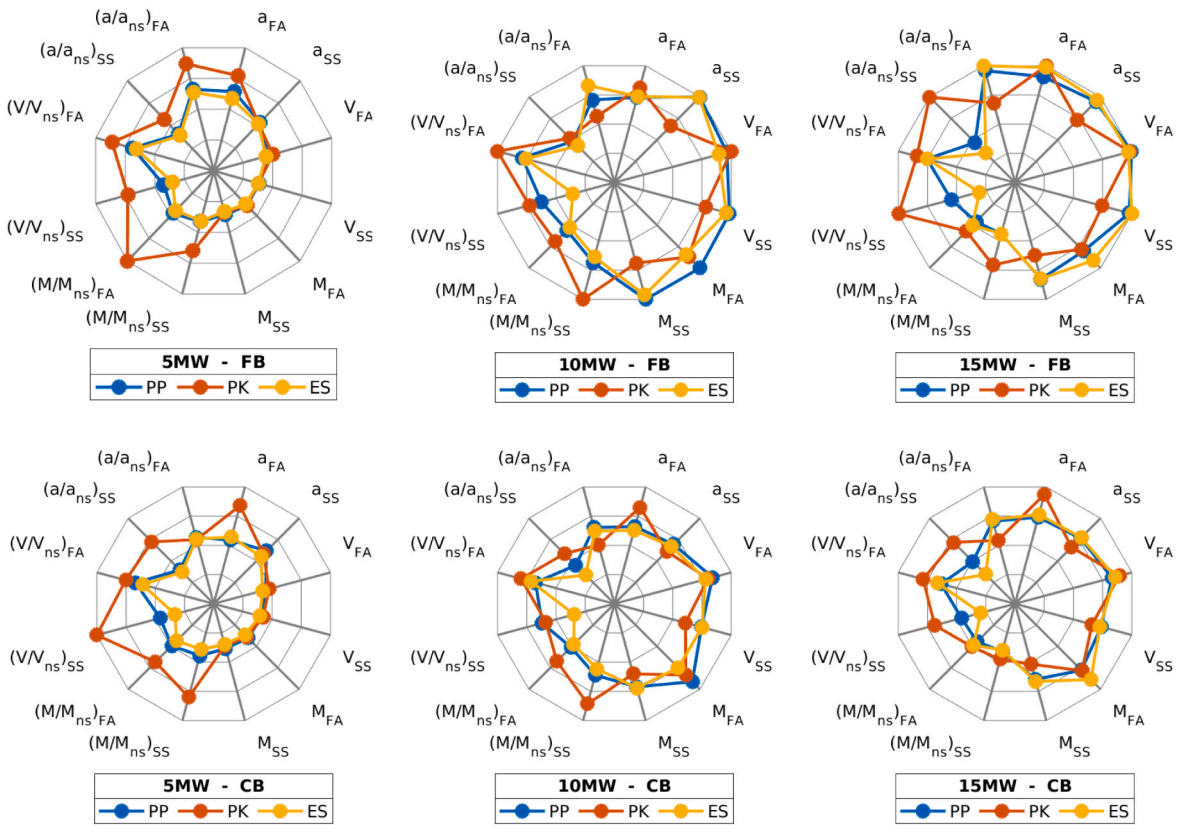

Fig. 15. Influence of the mode of operation. (a = Acceleration; M = Mudline Moment; V = Mudline shear force; NS = Absence of seismic input). The first subdivision of every radii is always 0. The axes limits is the same in all web plots in this figure to allow comparison. (For interpretation of the references to colour in this figure legend, the reader is referred to the web version of this article.)

into the general trends of the problem taking the dynamic soil–structure interaction phenomena into account. More detail seismic analyses of particular cases would benefit from introducing the non-linear response of the soil into the model.

CRediT authorship contribution statement

Luis A. Padrón: Conceptualization, Methodology, Software, Validation, Formal analysis, Investigation, Data curation, Writing - original draft, Writing – review & editing, Visualization, Supervision, Funding acquisition. **Sandro Carbonari:** Conceptualization, Methodology, Validation, Formal analysis, Investigation, Data curation, Writing - original draft, Writing - review & editing, Visualization. **Francesca Dezi:** Resources, Formal Analysis, Writing - original draft, Writing - review & editing. **Michele Morici:** Methodology, Resources, Writing - review & editing. **Jacob D.R. Bordón:** Resources, Writing - original draft, Writing - review & editing. **Graziano Leoni:** Conceptualization, Validation, Writing - review & editing.

Declaration of competing interest

The authors declare that they have no known competing financial interests or personal relationships that could have appeared to influence the work reported in this paper.

Acknowledgements

This study was supported by the Consejería de Economía, Conocimiento y Empleo (Agencia Canaria de la Investigación, Innovación y Sociedad de la Información) of the Gobierno de Canarias and FEDER through research project ProID2020010025, and by the Ministerio de Ciencia, Innovación y Universidades and the Agencia Estatal de Investigación of Spain, and FEDER, through research project BIA2017-88770-R. It was also supported by the Ministerio de Ciencia, Innovación y Universidades through the grant PRX19/00392 awarded to L.A. Padrón for a research stay at Università Politecnica delle Marche. Additional support was obtained from the program of support for research of the Universidad de Las Palmas de Gran Canaria through project ULPGC2018-11.

References

Álamo, G.M., Aznárez, J.J., Padrón, L.A., Martínez-Castro, A.E., Gallego, R., Maeso, O., 2018. Dynamic soil-structure interaction in offshore wind turbines on monopiles in layered seabed based on real data. Ocean Eng. 156, 14–28.

Alati, N., Failla, G., Arena, F., 2015. Seismic analysis of offshore wind turbines on bottom-fixed support structures. Phil. Trans. R. Soc. A 373.

Ali, A., De Risi, R., Sextos, A., Goda, K., Chang, Z., 2020. Seismic vulnerability of offshore wind turbines to pulse and non-pulse records. Earthq. Eng. Struct. Dyn. 49 (1), 24–50.

Alpan, I., 1970. The geotechnical properties of soils. Earth-Sci. Rev. 6 (1), 5–49.

Anastasopoulos, I., Theofilou, M., 2016. Hybrid foundation for offshore wind turbines: Environmental and seismic loading. Soil Dyn. Earthq. Eng. 80, 192–209.

Andersen, L.V., Vahdatirad, M.J., Sichani, M.T., Sørensen, J.D., 2012. Natural frequencies of wind turbines on monopile foundations in clayey soils - A probabilistic approach. Comput. Geotech. 43, 1–11.

Aranuvachapun, S., 1987. Parameters of JONSWAP spectral model for surface gravity waves—II. Predictability from real data. Ocean Eng. 14 (2), 101–115.

Asareh, M.-A., Prowell, I., Volz, J., Schonberg, W., 2016a. A computational platform for considering the effects of aerodynamic and seismic load combination for utility scale horizontal axis wind turbines. Earthq. Eng. Eng. Vib. 15 (1), 91–102.

Asareh, M.-A., Schonberg, W., Volz, J., 2015. Effects of seismic and aerodynamic load interaction on structural dynamic response of multi-megawatt utility scale horizontal axis wind turbines. Renew. Energy 86, 49–58.

Asareh, M.-A., Schonberg, W., Volz, J., 2016b. Fragility analysis of a 5-MW NREL wind turbine considering aero-elastic and seismic interaction using finite element method. Finite Elem. Anal. Des. 120, 57–67.

Bartolotti, P., Canet Tarres, H., Dykes, K., Merz, K., Sethuraman, L., Verelst, D., Zahle, F., 2019. IEA Wind Task 37 on Systems Engineering in Wind Energy – WP2.1 Reference Wind Turbines. techreport NREL/TP-73492, International Energy Agency, https://github.com/IEAWindTask37/IEA-10.0-198-RWT.

Bazeos, N., Hatzigeorgiou, G.D., Hondros, I.D., Karamaneas, H., Karabalis, D.L., Beskos, D.E., 2002. Static, seismic and stability analyses of a prototype wind turbine steel tower. Eng. Struct. 24, 1015–1025.

Bhattacharya, S., Adhikari, S., 2011. Experimental validation of soil-structure interaction of off-shore wind turbines. Soil Dyn. Earthq. Eng. 31, 805–816.

Bhattacharya, S., Goda, K., 2016. Use of offshore wind farms to increase seismic resilience of nuclear power plants. Soil Dyn. Earthq. Eng. 80, 65–68.

Bisoi, S., Haldar, S., 2014. Dynamic analysis of offshore wind turbine in clay considering soil-monopile-tower interaction. Soil Dyn. Earthq. Eng. 63, 19–35.

Bordón, J.D.R., 2017. Coupled Model of Finite Elements and Boundary Elements for the Dynamic Analysis of Buried Shell Structures (Ph.D. thesis). Universidad de Las Palmas de Gran Canaria.

Bordón, J.D.R., Aznárez, J.J., Maeso, O., 2017. Dynamic model of open shell structures buried in poroelastic soils. Comput. Mech. 60, 269–288.

Bucalem, M.L., Bathe, K.J., 1993. Higher-order MITC general shell elements. Internat. J. Numer. Methods Engrg. 36, 3729–3754.

Carbonari, S., Morici, M., Dezi, F., Leoni, G., 2018. A lumped parameter model for time-domain inertial soil-structure interaction analysis of structures on pile foundations. Earthq. Eng. Struct. Dyn. 47 (11), 2147–2171.

Carswell, W., Arwade, S.R., Degroot, D.J., Lackner, M.A., 2015a. Soil-structure reliability of offshore wind turbine monopile foundations. Wind Energy 17 (18), 483–498.

Carswell, W., Johansson, J., Løvholt, F., Arwade, S.R., Madshus, C., DeGroot, D.J., Myers, A.T., 2015b. Foundation damping and the dynamics of offshore wind turbine monopiles. Renew. Energy 80, 724–736.

Chopra, A.K., 2017. Dynamics of Structures. Theory and Applications to Earthquake Engineering, seventh ed. Pearson.

Damgaard, M., Andersen, L.V., Ibsen, L.B., 2014a. Computationally efficient modelling of dynamic soil-structure interaction of offshore wind turbines on gravity footings. Renew. Energy 68, 289–303.

Damgaard, M., Andersen, L., Ibsen, L., 2015a. Dynamic response sensitivity of an offshore wind turbine for varying subsoil conditions. Ocean Eng. 101, 227–234.

Damgaard, M., Andersen, L.V., Ibsen, L.B., Toft, H.S., Sorensen, J.D., 2015b. A probabilistic analysis of the dynamic response of monopile foundations: Soil variability and its consequences. Probab. Eng. Mech. 41, 46–59.

Damgaard, M., Bayat, M., Andersen, L.V., Ibsen, L.B., 2014b. Assessment of the dynamic behaviour of saturated soil subjected to cyclic loading from offshore monopile wind turbine foundations. Comput. Geotech. 61, 116–126.

Damgaard, M., Ibsen, L.B., Andersen, L.V., Andersen, J.K.F., 2013. Cross-wind modal properties of offshore wind turbines identified by full scale testing. J. Wind Eng. Ind. Aerodyn. 116, 94–108.

Damiani, R., Jonkman, J., Hayman, G., 2015. SubDyn User'S Guide and Theory Manual. techreport NREL/TP-5000-63062, National Renewable Energy Laboratory.

De Risi, R., Bhattacharya, S., Goda, K., 2018. Seismic performance assessment of monopile-supported offshore wind turbines using unscaled natural earthquake records. Soil Dyn. Earthq. Eng. 109, 154–172.

Díaz, O., Suárez, L.E., 2014. Seismic analysis of wind turbines. Earthq. Spectra 30 (2), 743–765.

DNV, 2014. Design of Offshore Wind Turbine Structures. Offshore Standard DNV-OS-J101. DetNorske Veritas AS.

European Committee for Standardization, 2005. EN 1998-1: 2005 eurocode 8: Design of structures for earthquake resistance. Part 1: General rules, seismic action and rules for buildings.

EWEA, 2020. Offshore Wind in Europe - Key Trends and Statistics 2019. Wind Europe.

Gaertner, E., Rinker, J., Sethuraman, L., Zahle, F., anderson, B., Barter, G., Abbas, N., Meng, F., Bartolotti, P., Skrzypinski, W., Scott, G., Fel, R., Bredmose, H., Dykes, K., Sheilds, M., Allen, C., Viselli, A., 2020. Definition of the IEA 15 MW Offshore Reference Wind Turbine. techreport NREL/TP-75698, International Energy Agency, https://github.com/IEAWindTask37/IEA-15-240-RWT.

Gasparini, D.A., Venmarcke, E.H., 1976. Evaluation of Seismic Safety of Buildings – Simulated Earthquake Motions with Prescribed Response Spectra. techreport 2, Massachusetts Institute of Technology.

Ghaemmaghami, A.R., Mercan, O., Kianoush, R., 2017. Seismic soil-structure interaction analysis of wind turbines in frequency domain. Wind Energy 20, 125–142.

González, F., Padrón, L.A., Carbonari, S., Morici, M., Aznárez, J.J., Dezi, F., Leoni, G., 2019. Seismic response of bridge piers on pile groups for different soil damping models and lumped parameter representations of the foundation. Earthq. Eng. Struct. Dyn. 48 (3), 306–327.

Harte, M., Basu, B., Nielsen, S.R.K., 2012. Dynamic analysis of wind turbines including soil-structure interaction. Eng. Struct. 45, 509–518.

Hofmann, M., Sperstad, I.B., 2014. Will 10 MW wind turbines bring down the operation and maintenance cost of offshore wind farms? Energy Procedia 53, 231–238, EERA DeepWind' 2014, 11th Deep Sea Offshore Wind R&D Conference.

IEC, 2005. 61400-1:2005 Wind Turbines - Part 1: Design Requirements. International Electrotechnical Commission.

ISO 19901-2, 2007. International organization for standardization. ISO 19901-2:2017 petroleum and natural gas industries — Specific requirements for offshore structures — Part 2: Seismic design procedures and criteria.

ISO 19902, 2007. International organization for standardization. ISO 19902:2007 petroleum and natural gas industries — Fixed steel offshore structures.

Jonkman, B.J., 2009. Turbsim User's Guide: version 1.50. techreport NREL/TP-500-46198, National Renewable Energy Laboratory.

Jonkman, J., Musial, W., 2010. Offshore Code Comparison Collaboration (OC3) for IEA Task 23 Offshore Wind Technology and Deployment. techreport NREL/TP-5000-48191, National Renewable Energy Laboratory.

Ju, S.-H., Huang, Y.-C., 2019. Analyses of offshore wind turbine structures with soil-structure interaction under earthquakes. Ocean Eng. 187, 106190.

Katsanos, E.I., Thöns, S., Georgakis, C.T., 2016. Wind turbines and seismic hazard: A state-of-the-art review. Wind Energy 19 (11), 2113–2133.

Kim, D.H., Lee, S.G., Lee, I.K., 2014. Seismic fragility analysis of 5MW offshore wind turbine. Renew. Energy 65, 250–256.

Kitahara, M., Ishihara, T., 2020. Prediction of seismic loadings on wind turbine support structures by response spectrum method considering equivalent modal damping of support structures and reliability level. Wind Energy 23 (6), 1422–1443.

Kjørlaug, R.A., Kaynia, A.M., 2015. Vertical earthquake response of megawatt-sized wind turbine with soil-structure interaction effects. Earthq. Eng. Struct. Dyn. 44 (13), 2341–2358.

Lavassas, I., Nikolaidis, G., Zervas, P., Efthimiou, E., Doudoumis, I.N., Baniotopoulos, C.C., 2003. Analysis and design of the prototype of a steel 1-MW wind turbine tower. Eng. Struct. 25, 1097–1106.

Løken, I.B., Kaynia, A.M., 2019. Effect of foundation type and modelling on dynamic response and fatigue of offshore wind turbines. Wind Energy 22 (12), 1667–1683.

Lombardi, D., Bhattacharya, S., Wood, D.M., 2013. Dynamic soil–structure interaction of monopile supported wind turbines in cohesive soil. Soil Dyn. Earthq. Eng. 49, 165–180.

Mardfekri, M., Gardoni, P., 2013. Probabilistic demand models and fragility estimates for offshore wind turbine support structures. Eng. Struct. 52, 478–487.

Mardfekri, M., Gardoni, P., 2015. Multi-hazard reliability assessment of offshore wind turbines. Wind Energy 18 (8), 1433–1450.

Meng, J., Dai, K., Zhao, Z., Mao, Z., Camara, A., Zhang, S., Mei, Z., 2020. Study on the aerodynamic damping for the seismic analysis of wind turbines in operation. Renew. Energy 159, 1224–1242.

Mo, R., Kang, H., Li, M., Zhao, X., 2017. Seismic fragility analysis of monopile offshore wind turbines under different operational conditions. Energies 10, 1037.

Morici, M., Minnucci, L., Carbonari, S., Dezi, F., Leoni, G., 2019. Simple formulas for estimating a lumped parameter model to reproduce impedances of end-bearing pile foundations. Soil Dyn. Earthq. Eng. 121, 341–355.

OpenFAST Documentation, 2020. Release v2.3.0. National Renewable Energy Laboratory, https://openfast.readthedocs.io/en/master/. Code published at https://github.com/OpenFAST/openfast.

Prowell, I., 2011. An Experimental and Numerical Study of Wind Turbine Seismic Behavior (Ph.D. thesis). University of California, San Diego, CA, USA.

Prowell, I., Elgamal, A., Uang, C.-M., Enrique Luco, J., Romanowitz, H., Duggan, E., 2014. Shake table testing and numerical simulation of a utility-scale wind turbine including operational effects. Wind Energy 17 (7), 997–1016.

Sadowski, A.J., Camara, A., Málaga-Chuquitaype, C., Dai, K., 2017. Seismic analysis of a tall metal wind turbine support tower with realistic geometric imperfections. Earthq. Eng. Struct. Dyn. 46 (2), 201–219.

Santangelo, F., Failla, G., Santini, A., Arena, F., 2016. Time-domain uncoupled analyses for seismic assessment of land-based wind turbines. Eng. Struct. 123, 275–299.

Song, B., Yi, Y., Wu, J., 2013. Study on seismic dynamic response of offshore wind turbine tower with monopile foundation based on M method. Adv. Mater. Res. 663, 686–691.

Stamatopoulos, G.N., 2013. Response of a wind turbine subjected to near-fault excitation and comparison with the greek aseismic code provisions. Soil Dyn. Earthq. Eng. 46, 77–84.

Taddei, F., Schauer, M., Meinerzhagen, L., 2017. A practical soil-structure interaction model for a wind turbine subjected to seismic loads and emergency shutdown. Procedia Eng. 199, 2433–2438, X International Conference on Structural Dynamics, EURODYN 2017.

Valamanesh, V., Myers, A.T., 2014. Aerodynamic damping and seismic response of horizontal axis wind turbine towers. J. Struct. Eng. 140 (11).

Velarde, J., Bachynski, E.E., 2017. Design and fatigue analysis of monopile foundations to support the DTU 10 MW offshore wind turbine. Energy Procedia 137, 3–13, 14th Deep Sea Offshore Wind R&D Conference, EERA DeepWind'2017.

Wang, L., Dong, X., 2011. Influence of earthquake directions on wind turbine tower under seismic action. Adv. Mater. Res. 243–249, 3883–3888.

Wang, L., Zhang, Y., 2011. Influence of simplified models on seismic response analysis of wind turbine towers. Appl. Mech. Mater. 94–96, 369–374.

Yang, Y., Bashir, M., n, C.L., Wang, J., 2019a. Analysis of seismic behaviour of an offshore wind turbine with a flexible foundation. Ocean Eng. 178, 215–228.

Yang, Y., Li, C., Bashir, M., Wang, J., Yang, C., 2019b. Investigation on the sensitivity of flexible foundation models of an offshore wind turbine under earthquake loadings. Eng. Struct. 183, 756–769.

Zania, V., 2014. Natural vibration frequency and damping of slender structures founded on monopiles. Soil Dyn. Earthq. Eng. 59, 8–20.